LITHOS

New insight from plumbing system below composite mafic volcanoes: post-glacial volatile contents and magmatic fluids from Villarrica magmas

--Manuscript Draft--

Manuscript Number:	LITHOS12050
Article Type:	Regular Article
Keywords:	Villarrica volcano, Polygenetic system, Melt inclusions, Pre-eruptive Volatiles, Mafic Plinian Volcanism
Corresponding Author:	Philippe Robidoux, Ph.D. University of Chile Santiago, CHILE
First Author:	Philippe Robidoux, Ph.D.
Order of Authors:	Philippe Robidoux, Ph.D.
	Yves Moussallam
	Estelle F. Rose-Koga
	Andrea Luca Rizzo
	Guillaume Georgeais
	Joao Lages
	Gilles Lévresse
	Simona Ferrando
	Alessandro Aiuppa
Abstract:	Composite volcanoes are complex geological systems characterised by efficient transport of magma both vertically and laterally to the Earth's surface, producing a variety of volcanic hazards. There are relatively few examples of volcanoes with mafic explosive volcanic activity, such as the Masaya volcano in Nicaragua and the Tongariro volcano in New Zealand. The Villarrica volcano in the southern Andes of Chile, which formed during the Andean deglaciation period, also falls into this category. Its building phase was punctuated by the creation of a collapsed caldera some 14.5 to 13.5 ka during the Licán ignimbrite event. Following glacial retreat, volatile-saturated magma originating from a depth of 14.4 to 17 km below Villarrica introduced CO2-rich melt into the central crater, an eruptive event known as the Pucón ignimbrite. The Los Nevados Minor Eruptive Centers (MECs) served as conduits facilitating the lateral transport of degassing magmas at similar depths (14.2–21.3 km) traversing the Caldera 1 structure and having co-genetic compositions, while the Chaillupén MECs represented a field closer to the central crater, also a degassing end member magma from a smaller depth range (0.3–6.8 km). Another structure, the Caburgua monogenetic cone, situated beyond the confines of the Villarrica volcanic complex, was fed by degassed melt from a depth of 17 km. Although this magma has trace element ratios similar to those of the Caburgua-Huellemolle MECs, it has distinctive modifications attributable to asthenospheric slab fluid melts that distinguish it from that of the Villarrica stratovolcano. We estimated the minimum pressure required for volatile saturation in Villarrica magmas (<5.9 kb) by analyzing the CO2 contents in 167 naturally quenched melt inclusions hosted in olivine phenocrysts. We found typical shrinkage bubbles of less than 6% by volume and measured micro-Raman densities ranging from 0.012 to 0.778 grams per cubic centimetres, as well as solubility models based on autocorrelated micro-FTIR and SIMS measurements on glassy inclusions. These findings suggest that the Pucón eruption recorded the highest uncorrected volatile contents, including 6.0 wt.% H2O, over 1500 ppm CO2, 1330 ppm S, 1556 ppm Cl, and 2055 ppm F. Helium isotope ratios (3He/4He; Rc/Ra when corrected for atmosphere) measured in bulk noble gases from olivines (Fo75–88) indicate that the parental magmatic fluid signature (Rc/Ra = 6.7–7.6; CO2/3He = 4.7–7.5E+08) is only recorded during paroxysmal eruptions, and that this primitive gas signal is diluted in lateral MECs (Rc/Ra<6.5; CO2/3He = 1.4x10+9–3.1x10+10), confirming new findings

on the lateral dispersion of magmatic fluids within polygenetic volcano systems. Bulk rock trace and REE ratios also indicate that peripheral vents are fed by intermediate compositions derived from parental MORB magmas, showing assimilation of slab-fluid sediment input, in addition to being contaminated to varying degrees by lithospheric elements. The ascending Pucón magma is interpreted to have fragmented and assimilated Cenozoic plutonic rocks towards the end of its eruptive sequence, while the Chaimilla magma (3.1 ky) traversed the same continental basement at a depth of over 4.4 km. Chaimilla represents a cogenetic melt from Pucón but is H_2O-CO_2 depleted (2.6wt.%-409 ppm). Its magma was channeled through the same conduits as the present Villarrica volcano (minimum depth of 1.7 km to become volatile saturated). The increase in lithospheric contamination over time is confirmed by bulk rock chemistry using REE ratios sensitive to lithospheric contamination (Rb/Sr; Sr/Y) and slab fluid sediment assimilation (Th/Nb; Sr/Nd; Th/La; La/Sm). Taken together, these empirical observations reveal the intricate workings of a polygenetic volcano and highlight that, despite the input of successive mafic magma batches, the parent magmas beneath composite volcanic systems such as Villarrica can facilitate the transport of variably degassed magmas. These magmas can show both temporal and spatial variations, resulting in the formation of different volcanic vents on their flanks.

Suggested Reviewers:	George Zellmer G.F.Zellmer@massey.ac.nz Expert of volatile studies in subduction settings and dedicated to volcanic hazard mitigation.
	John Stix john.stix@mcgill.ca Internationally recognized volcanologist who treated several studies of degassing mafic magmatic systems.
	Jeffrey Witter jeff@innovategeothermal.co Geologist who completed his PhD thesis and work on the venting system of the Villarrica volcano, covering various aspects of geochemical studies of the system during the 2000s.
	Takeshi Kuritani Hokkaido University Faculty of Science kuritani@sci.hokudai.ac.jp Expert on studies of magmatic processes in similar active volcanoes, where experimental and geochemical tools have helped to assess magma genesis as a characterisation of magmatic differentiation for basalt-to-andesitic melt compositions.
Opposed Reviewers:	

« New insight from plumbing system below composite mafic volcanoes: post-glacial volatile contents and magmatic fluids from Villarrica magmas »

Author names and affiliations: Philippe Robidoux[a], Yves Moussallam[b,c], Estelle F. Rose-Koga[d], Andrea Luca Rizzo[e,f], Guillaume Georgeais[b], Joao Lages[g,h], Gilles Lévresse[i], Simona Ferrando[j], Alessandro Aiuppa[g,h]

[a] Department of Geology, Facultad de Ciencias Físicas y Matemáticas, Universidad de Chile, 8370450 Santiago, Chile

[b]Lamont-Doherty Earth Observatory, Columbia University, New York, USA

[c]American Museum of Natural History, Department of Earth and Planetary Sciences, NY 10024, New York, USA

[d]Institut des Sciences de la Terre d'Orléans (ISTO), CNRS UMR 7327, Université d'Orléans, BRGM, 1A rue de la Férollerie, 45071 Orléans, Cedex 2, France

[e]University of Milano Bicocca, DIpartimento di Scienze Dell Ambiente e della Terra (DISAT), Milano, Italy

[f]Istituto Nazionale di Geofisica e Vulcanologia (INGV), Sezione di Milano, Milano, Italy, Via Alfonso Corti, 12, 20133 Milano MI

[g]Dipartimento DiSTeM, Universitá degli Studi di Palermo, Palermo, Italy

[h]Istituto Nazionale di Geofsica e Vulcanologia (INGV), Sezione di Palermo, Via Ugo La Malfa 153, 90146, Palermo, Italy

[i]Centro de Geociencias, UNAM Campus Juriquilla Blvd. Juriquilla 3001, Querétaro 76230, Mexico

[j]Simona Ferrando, Department of Earth Sciences, University of Torino, Via Valperga Caluso 35,10125, Torino, Italy

Corresponding author.

Dr. Philippe Robidoux

Department of Geology, Facultad de Ciencias Físicas y Matemáticas, Universidad de Chile, Plaza Ercilla 803, 8370450, Santiago, Chile

E-mail address: robidouxphilippe@gmail.com

Santiago, January 30, 2024

Lithos Editorial Board
Section Editor-in-Chief

Dear Editor,

I am writing to submit the manuscript titled "**New insight from plumbing system below composite mafic volcanoes: post-glacial volatile contents and magmatic fluids from Villarrica magmas**" by Robidoux et al. for consideration as a Regular Article in the Journal of Lithos.

In this study, we present compelling evidence from petrogenesis, magma and volatile chemistry that confirms multiple magma transport conditions and the source of a basaltic andesite composite volcano. Our results shed new light on the Villarrica volcano, located in the Southern Volcanic Zone (SVZ) of the Andes.

Key contributions of our research include:

1. At Villarrica volcano since post-glacial period-to present, the Pucón ignimbrite represent the best-preserved inclusion products and closer in composition to parental mantle-derived magma according to volatiles (H_2O, CO_2, S, Cl, F) major element composition from melt inclusions and their variation in typical post entrapment crystallization characteristics observed in olivines. Subsequent mafic magma recharges are compositionally derived from Pucón ignimbrite.

2. Integration of petrological data with pressure and temperature conditions (~< 1200 °C, ~< 45 km equivalent crustal depth) of post-glacial magmatic events is performed for the first time at Villarrica for multiple eruptive events, estimated using volatile solubility models based on mRaman CO_2 correction considering shrinkage bubbles of olivine hosted melt inclusions.

3. Sequential measurement of noble gas (He-Ne-Ar) isotopic compositions of fluid inclusions trapped in olivines from Holocene to post-glacial volcanic rock of Villarrica volcano. We report a magmatic $^3He/^4He$ signature of 7.6 Ra, within the MORB range (8±1 Ra), values only reached during paroxysmal eruptions.

4. Analysis of bulk rock chemistry from minor eruptive centres (MEC) on the flank of Villarrica reveal that parental magmas are generated by the incorporation of continental contamination, slab-rich fluids with low sediment input. This characteristic decreases spatially in flank MECs and monogenetic Caburgua.

The identification of these geochemical features, carried out in detail and in chronological order, finally sheds light on the eruptive paroxysm driven by mafic magmas in composite volcanic systems such as Villarrica. Evidence is provided that polygenetic volcanism infiltrates a variety of mafic magma inputs from parent magmas. These results provide powerful tools for understanding natural volcanic hazards.

This work and the data presented are original and were never published elsewhere. I look forward to hearing from you.

Best regards,

Philippe Robidoux

Via Ersilia 803, Santiago, Chile – Tel. +56951232150 –
e-mail: robidouxphilippe@gmail.com

Abstract

Composite volcanoes are complex geological systems characterised by efficient transport of magma both vertically and laterally to the Earth's surface, producing a variety of volcanic hazards. There are relatively few examples of volcanoes with mafic explosive volcanic activity, such as the Masaya volcano in Nicaragua and the Tongariro volcano in New Zealand. The Villarrica volcano in the southern Andes of Chile, which formed during the Andean deglaciation period, also falls into this category. Its building phase was punctuated by the creation of a collapsed caldera some 14.5 to 13.5 ka during the Licán ignimbrite event. Following glacial retreat, volatile-saturated magma originating from a depth of 14.4 to 17 km below Villarrica introduced CO_2-rich melt into the central crater, an eruptive event known as the Pucón ignimbrite. The Los Nevados Minor Eruptive Centers (MECs) served as conduits facilitating the lateral transport of degassing magmas at similar depths (14.2–21.3 km) traversing the Caldera 1 structure and having co-genetic compositions, while the Chaillupén MECs represented a field closer to the central crater, also a degassing end member magma from a smaller depth range (0.3–6.8 km). Another structure, the Caburgua monogenetic cone, situated beyond the confines of the Villarrica volcanic complex, was fed by degassed melt from a depth of 17 km. Although this magma has trace element ratios similar to those of the Caburgua-Huellemolle MECs, it has distinctive modifications attributable to asthenospheric slab fluid melts that distinguish it from that of the Villarrica stratovolcano. We estimated the minimum pressure required for volatile saturation in Villarrica magmas (<5.9 kb) by analyzing the CO_2 contents in 167 naturally quenched melt inclusions hosted in olivine phenocrysts. We found typical shrinkage bubbles of less than 6% by volume and measured micro-Raman densities ranging from 0.012 to 0.778 grams per cubic centimetres, as well as solubility models based on autocorrelated micro-FTIR and SIMS measurements on glassy inclusions. These findings suggest that the Pucón eruption recorded the highest uncorrected volatile contents, including 6.0 wt.% H_2O, over 1500 ppm CO_2, 1330 ppm S, 1556 ppm Cl, and 2055 ppm F. Helium isotope ratios ($^3He/^4He$; Rc/Ra when corrected for atmosphere) measured in bulk noble gases from olivines ($Fo_{75–88}$) indicate that the parental magmatic fluid signature (Rc/Ra = 6.7–7.6; $CO_2/^3He$ = 4.7–7.5E^{+08}) is only recorded during paroxysmal eruptions, and that this primitive gas signal is diluted in lateral MECs (Rc/Ra<6.5; $CO_2/^3He$ = 1.4x10^{+9}–3.1x10^{+10}), confirming new findings on the lateral dispersion of magmatic fluids within polygenetic volcano systems. Bulk rock trace and REE ratios also indicate that peripheral vents are fed by intermediate compositions derived from parental MORB magmas, showing assimilation of slab-fluid sediment input, in addition to being contaminated to varying degrees by lithospheric elements. The ascending Pucón magma is interpreted to have fragmented and assimilated Cenozoic plutonic rocks towards the end of its eruptive sequence, while the Chaimilla magma (3.1 ky) traversed the same continental basement at a depth of over 4.4 km. Chaimilla represents a cogenetic melt from Pucón but is H_2O-CO_2 depleted (2.6wt.%-409 ppm). Its magma was channeled through the same conduits as the present Villarrica volcano (minimum depth of 1.7 km to become volatile saturated). The increase in lithospheric contamination over time is confirmed by bulk rock chemistry using REE ratios sensitive to lithospheric contamination (Rb/Sr; Sr/Y) and slab fluid sediment assimilation (Th/Nb; Sr/Nd; Th/La; La/Sm). Taken together, these empirical observations reveal the intricate workings of a polygenetic volcano and highlight that, despite the input of successive mafic magma batches, the parent magmas beneath composite volcanic systems such as Villarrica can facilitate the transport of variably degassed magmas. These magmas can show both temporal and spatial variations, resulting in the formation of different volcanic vents on their flanks.

Keywords

Villarrica volcano, Polygenetic system, Melt inclusions, Pre-eruptive Volatiles, Mafic Plinian Volcanism

Highlights

- Villarrica is a polygenetic volcanic system of the South Volcanic Zone.
- Inclusion-mineral chemistry identifies postglacial mafic parent magma.
- Polybaric crystal fractionation and degassing of volatiles below 17 km.
- Villarrica fluids reveal spatial decrease in crustal contamination.
- Paroxysmal explosive eruptions conserve primitive MORB-like signature of $^{3}He/^{4}He$

1. Introduction

Composite stratovolcanoes have a central vent that is fed by basaltic magma, and their flanks are dotted with minor eruptive centers (MECs), which give rise to hazards across a broader zone. Villarrica is an active open vent volcano in the Southern Andes Volcanic Zone (SVZ), which formed as a consequence of the subduction of the 12–20 My-old Nazca plate beneath the South American plate (Jarrard, 1986; Stern, 2004). Villarrica typically produces Strombolian/Hawaiian volcanic activity occurring at central as well as lateral volcanic vents but has also produced Vulcanian to sub-Plinian eruptions (Silva et al., 2010; Costantini et al., 2011; Lohmar et al., 2012) and mafic ignimbritic eruptions (Moreno and Clavero, 2006). The source and location of these magmatic recharge bodies remains poorly constrained, but the mechanism has been documented in volcanoes with similar mafic magma ascent (Moitra et al., 2018 and references therein). Villarrica volcano, located at 39°24'S and 71°55'W (Fig. 1a), hosts an active lava lake (e.g., Witter et al., 2004; Moussallam et al, 2016, 2023). The main explosive eruption hazard stems from its central vent (e.g. Santiago pit crater, Masaya, Stix et al., 1998), but could also involve multiple synchronous vents during paroxysmal explosive events (e.g., Mt. Tongariro, New Zealand, Heinrich et al., 2020). The distribution of effusive activity on the flanks of stratovolcanoes is also of concern, as postglacial volcanostratigraphy indicates frequent outbursts of voluminous lava flows accompanied by small explosive eruptions, resulting in the formation of spreading clusters of MECs (Moreno and Clavero, 2006). In the light of these natural hazards, there are two major petrogenetical problems to be addressed concerning stratovolcano systems dominated by mafic magma replenishment, such as Villarrica:

1. **Temporal depth evolution of magmas and pre-eruptive conditions:** Understanding the evolution and origin of the basaltic andesitic magma identified within the actual morphostructural context of Villarrica volcano (Moreno and Clavero, 2006), which produces Strombolian to subplinian activity requires an examination of pre-eruptive conditions (e.g., Cassidy et al., 2018). On the basis that volatiles are key to interpreting eruptive style and explosivity at volcanic centers (Cashman, 2004), we examine whether evidence from magma and gas compositions can reveal a temporal evolution of magma composition and transport conditions within the plumbing system at Villarrica.

2. **Source and spatial distribution of magmatic fluids and volatiles:** The magma reservoirs feeding the composite Villarrica "polygenetic" system involve a diverse, overlapping system of plumbing levels and magma compositions (Geiger et al, 2018). The formation of mafic flank MECs and/or volcanism may produce a wide range of magma geochemistry resulting from the complex transport history in the Villarrica area (Valentine et al., 2015; Smith and Németh, 2017). Examples of these are the pyroclastic cones and associated lavas of Caburgua-Huelemolle Small Eruptive Centers (CHSEC), located in the southern sector of lake Caburgua, a few kilometers northeast of the Villarrica stratovolcano, with an estimated age of 9,000 yr B.P. (Moreno and Clavero, 2006). Thus, the second challenge at Villarrica is to determine whether degassing processes are driven by the same magmatic fluids, across the post-glacial regional edifices (MECs), and the flank volcanic

centers that have formed in the current 2 km-wide caldera (Villarrica Unit 3, <~ 3.7 Kyr AP; Moreno and Clavero, 2006).

Stratigraphic mapping at Villarrica over the last few decades has led to an improved model of the eruptive sequence (Moreno and Clavero 2006), while the development of seismic and gas monitoring techniques has helped understand the present state of volcanic activity (Lehr et al., 2022 and references therein). Here, we investigate the pre-eruptive conditions of the post-glacial magmatic ascent history, using melt inclusions (MIs; e.g., Wallace et al., 2021) to characterize the chemistry of the magmatic fluids associated with eruptive products coming from a deeper source in the volcano-magmatic plumbing system. Melt inclusion compositions from olivine crystals complement bulk rock analyses to illustrate detailed degassing and differentiation mechanisms occurring at various feeder system locations and intrusive stages from the polygenetic Villarrica volcanic system.

Villarrica has undergone eruptions of variably degassed magma evolving at shallow crustal depths, sourced from > 45 km depth in the MOHO-lithospheric mantle (Tassara and Echaurren, 2012; Hickey-Vargas et al., 2016). To define the source and spatial distribution of Villarrica's magmatic fluids and volatiles, we combine our MI study with a high-resolution isotopic noble gas fluid study on olivine crystals sampled at several regional MECs on the volcano flanks. Previous studies showed that $^{3}He/^{4}He$ measurements in olivine-hosted fluid inclusions from the 2015 Villarica eruption have an isotopic signature as high as 6.7 Ra (Lages et al., 2021b). This is still lower than the typical homogeneous Andean signature in the mantle along the South American Arc of 8–9 Ra (Lages et al., 2021a,b). Here, therefore, we investigate the causes of $^{3}He/^{4}He$ variations in magma batches generated at different MECs using the chronology of the most highly-studied explosive mafic paroxysms at Villarrica, which all fall within the post-glacial eruptive period.

2. Magmatic context and methodology

2.1 Tectonic context and post glacial magmatic background

Villarrica is part of the oblique Villarrica-Quetrupillán-Lanín chain in front of the Southern Volcanic Zone (SVZ). It is bounded by the Juan Fernandez Ridge at its northern edge (~33°S) and the Chile Rise to the south (~46°S) (Fig. 1 a). Volcanism in the Andes is the result of the subduction of the Nazca and Antarctic oceanic plates (45 My old) beneath the South American continental plate (Stern, 2004), which is moving obliquely (20–30°) to the NE a rate of 7–9 cm/yr (DeMets et al., 2001). The basement beneath the

Pleistocene-to-Holocene SVZ stratovolcanoes consists of continental crust which is ~ 35–60 km in thickness, above a shallowly dipping (< 25°) Benioff zone (Tassara and Echaurren, 2012). Where the mantle wedge is less well developed (~ 50 km thick), the overlying crust is much younger, with Paleozoic pre-Andean basement and Mesozoic-Cenozoic igneous rocks (Stern, 2004).

Villarrica volcano is close to densely populated urban and tourist areas, and has persistent degassing (e.g., Moussallam et al., 2016; Liu et al., 2019) and frequent effusive and explosive activity (Costantini et al., 2011). Petrological studies and the interpretation of seismic and geodetic data indicate a wide range of pre-eruptive magma storage conditions, in the range of 1.5–8 km in depth (Lohmar et al. 2012; Delgado et al., 2017; Lehr et al., 2022), while the crystallization of olivine-augite pair models indicating >7 kb pressure conditions (Boschetty et al., 2022). According to mineral-liquid geothermobarometry, the last Strombolian paroxysm, characterized by lava fountaining, may have been sourced from magma stored at a depth of 9.4–16.3 km and a Temperature around 1140 °C (Romero et al., 2022, Moussallam et al., 2023).

Three major evolutionary steps define the construction and collapse of Villarrica stratovolcano, with respect to past deglaciation ages (Moreno and Clavero, 2006; Watt et al., 2013). The occurrence of major VEI events has been identified from volcano stratigraphy and ^{14}C geochronology, from the oldest identified intra-glacial Pyroclastic Deposit of 40–14 ky to several post-glacial to Holocene events (Moreno and Clavero, 2006). The history associated with the development of the stratovolcano is divided into Villarrica units 1, 2, and 3, but the overall volatile data is very scarce, except for the Chaimilla fallout deposit produced from Unit 3 to the present-day (Pioli et al., 2015). We focus here on Unit 3 of Villarrica because it represents the series of volcanic layers that cover the current structure of Caldera 2 (Fig. 1b; Moreno and Clavero, 2006), which formed after the 14.5–13.5 ky BP (^{14}C date) Licán ignimbrite and reached a minimum depth of 1.5 km (6.8 kb) and marked the end of a major volcanic cycle at Villarrica (Lohmar et al., 2012).

2.2 Methodology

The major eruptive events have been studied through a series of new pyroclastic rocks sampled from Villarrica and the MECs (Table 1). The most well-documented explosive mafic eruptions at Villarrica were selected because they were produced chronologically after the Licán ignimbrite, so that we can focus on the syn- to postglacial context of the actual Villarrica edifice. The list of samples and analytical methods is given in Tables 1 and 2, with full details of the methodology given in Appendix A “Supplementary Material Methodology Review”.

2.2.1 Micro analytical approach for determining P-T-X magma conditions.

To understand magma evolution with depth and pre-eruptive conditions, we measured the major elements using electron microprobe analysis (EMPA) and volatile contents of naturally quenched olivine-hosted MIs with secondary ion microprobe spectrometry (SIMS) (e.g. volatile collection H_2O-CO_2-S-Cl-F) comparing with Fourier Transform Infrared microspectrometry (mFTIR) (e.g. dependent-pressure H_2O-CO_2 volatile pair). Quantitative parameters related to post-entrapment crystallization (PEC) are reported in Table 2 and Appendix B and the PEC correction procedure is detailed in Appendix A. The depth of magma evolution for each Villarrica magma sequence is determined using solubility models, taking into account the CO_2 in the shrinkage bubbles measured by µRaman (e.g. Robidoux et al., 2018) for the bubble-corrected CO_2 estimates. Petrographic characterization is applied to basalt-to basaltic andesite pyroclasts from central Villarrica and to regional MECs (including a potential monogenetic volcanic system, Caburgua cone #1; Caburgua-Huellemole Group). In all cases, the MIs provide a snapshot of the melt compositions during magma crystallization and/or degassing, which depends on transport conditions. The comprehensive dataset of olivine and major element measurements in melt inclusions, including information on volatile contents, is provided in Appendix A. This section encompasses a detailed account of the analytical approach, precision, and reproducibility for each method, along with complete instrument specifications.

2.2.2 Bulk analysis of whole rock and isotopic noble gases

To explore the source and spatial distribution of magmatic fluids and volatiles, eleven isotopic analyses of He-Ne-Ar were carried out in fluid inclusions (FIs) trapped in olivine crystals from the Villarica volcanic system at the laboratory of INGV, Sezione di Palermo (Italy). These measurements were combined with three other samples previously studied by Lages et al. (2021b), which are part of the same suite of samples. Those FIs occur within pyroclasts of mafic composition for each investigated eruptive event, and the whole-rock composition was also analyzed (Table 2, Appendix B). Approximately 0.1–1.2 g of unaltered crystals were hand-picked for noble gas analysis. After cleaning in an ultrasonic bath under nitric acid, acetone and deionised water, the crystals were loaded into a single-stage crusher and then baked under pumping to achieve ultra-high vacuum conditions. After crushing, the gas mixture released from the opening of the fluid inclusions was purified in a preparation system capable of separating noble gases from the main components, and then further separating helium from neon from argon (see Rizzo et al., 2018, 2022, Lages et al., 2021a, 2021b for further details).

Two distinct split-flight-tube mass spectrometers (Helix SFT-Thermo) were used to measure the isotopes of helium (^3He and ^4He) and ^{20}Ne, independently. The $^3He/^4He$ ratios are stated in R/Ra units, where Ra represents the $^3He/^4He$ of atmospheric air, which is 1.39×10^{-6}. The analytical error for the ^{20}Ne (1σ) was <0.8%. The He-isotope ratio measurements had an uncertainty (1σ) of less than 6%. According to Rizzo et al. (2018), the ^{20}Ne has been corrected for isobaric interferences at m/z values of 20 ($^{40}Ar^{2+}$). A multicollector mass spectrometer (GVI Argus) was used to measure the stable argon isotopes (^{36}Ar, ^{38}Ar, and ^{40}Ar) with an analytical uncertainty of $^{40}Ar/^{36}Ar$ < 0.2%. For the elemental and isotopic recalculations of He, Ne, and Ar, a pre-purified air standard separated into tanks was utilized. The standards for ^{4}He, $^{3}He/^{4}He$, ^{20}Ne and ^{40}Ar had analytical reproducibilities of less than 2.4%, 2.6%, 2.5% and 2.4%, respectively, over a period of >1 year for He and Ne and ~ 4 years for Ar. For He, Ne, and Ar, the typical blanks were at least two orders of magnitude lower than samples and standard signals. Additional information regarding sample preparation and analytical techniques can be found in Rizzo et al. (2018, 2022) and Lages et al. (2021a, 2021b).

Helium isotopic ratios are expressed as Rc/Ra, where Rc is the air-corrected $^{3}He/^{4}He$ ratio of the sample, determined using the $^{4}He/^{20}Ne$ ratios. The Rc/Ra value is equal to:

$[(R_m/R_a)(He/Ne)_m – (He/Ne)_{air}]/[(He/Ne)_m – (He/Ne)_{air}]$, where "m" and "air" denote air and measured values, respectively.

Because the argon concentration in the atmosphere is much higher than in magmatic fluid inclusions, it was necessary to make a correction, which assumes that all of the ^{36}Ar in the gas phase is atmospheric in origin. Thus, in the samples with $^{40}Ar/^{36}Ar$>300, the ^{40}Ar concentration can be corrected as follows:

$^{40}Ar^* = {}^{40}Arm-[(^{40}Ar/^{36}Ar)air\times{}^{36}Arm]$, where m is the measured value and $^{40}Ar^*$ is the corrected isotope value.

3. Results

3.1 Pyroclastic deposit classification and fragment size distribution

Sample collection and preparation for the study of volatiles in glassy inclusions (Lloyd et al., 2013) and olivine separation for bulk isotopic noble gas analyses (Robidoux et al., 2021) were carried out to select material below lapilli size granulometry. Both the pyroclasts of this size and the olivine mineral inclusions will have cooled rapidly, providing ideal trapping conditions for the inclusion in the host mineral and avoiding significant loss of H_2O due to H+ diffusion (Gaetani et al., 2012). The study covers all the pyroclastic deposits in both the monogenetic center, MECs and the adjacent Villarrica stratovolcano. At each site, ~5,000 grams of sample were sieved in the laboratory to retrieve the granulometric parameter and compared with datasets in the literature from Silva et al. (2010).

To compare the different volcanic deposits, the median weight was calculated for grain size distribution in pyroclastic flow deposits, surge, and fallout deposits (Table 1, and Appendix A). The Pucón ignimbrite data represents the initial fall deposit (TVP10E; Md = -1.547; σ = 1.449) and matches the onset of the “Pb” eruptive phase of the Pucón ignimbrite (Moreno & Clavero, 2006), preceding the ignimbrite pyroclastic flow sequence (P1, P2; Silva, 2010, and references therein). The extreme end member for well-sorted and small fragments is associated with the Chaimilla and Caburgua fallout deposits (TVP06 series; Md = -0.97 to 1.1; σ = -2.1 to -1.41). Los Nevados, Chaillupén and the March 2015 Villarrica volcanic episode all fall below -2 and -6 Mdφ (50), due to the sampling collection of single lapilli- to bomb-sized fragments.

3.2 Bulk rock geochemistry

The major element compositions of the bulk rock samples are presented in Appendix B. The Villarrica samples are heterogeneous at Pucón, ranging from basaltic to andesitic (SiO_2=52.1–61.9 wt.%, K_2O=0.52–1.47 wt.%, MgO=2.52–4.84 wt.%), homogeneous at Chaimilla (SiO_2=~53.1 wt.%, K_2O=0.57–0.61 wt.%, MgO=3.9–4.0 wt.%), and overlapping in SiO_2 concentration with the lava fountain scoria composition from 2015 (SiO_2=~53.1 wt.%, K_2O=0.77–0.86 wt.%, MgO=5.31–5.56 wt.%). The range of bulk rock compositions for MEC is restricted to basaltic andesites at Los Nevados (SiO_2=52.3–55.1 wt.%, K_2O=0.67–1.02 wt.%, MgO=4.10–4.47 wt.%) and Chaillupén (SiO_2=53.5–54.5 wt.%, K_2O=0.77–0.84 wt.%, MgO=4.84–5.07 wt.%), but strictly basaltic at Caburgua (SiO_2=50.8–51.9 wt.%, K_2O=0.67–0.75 wt.%, MgO=6.87–6.97 wt.%). The rocks are classified within the CA and HK-CA series fields (Fig. 2a).

The trace element compositions of the Villarrica rocks show a slight enrichment in light rare earth elements (LREEs), compared to the moderate and heavy rare earth elements, typical of MORB (Appendix C; Hickey-Vargas et al., 2016). The rocks are slightly enriched in large-ion lithophile elements (e.g., Cs, Rb, Sr, and Ba) relative to N-MORB, but overlap with E-MORB. Most samples have low contents of the high field strength elements (HFSE) Ta, Nb, Zr, and Hf.

3.3 Olivine texture, chemistry, and MI description

The group of olivine crystals from each eruptive event was characterized for its dominant MI textures by grouping all minerals as populations for each volcanic deposit (Appendix D). In this study, olivine hosted MI are referred to as "MI populations" when they are derived from the same layer of a volcanic deposit. The percentage variations of the MI typologies (Robidoux et al., 2018) are classified according to the "cooling rate-dependent" textural description of MI typologies of Roedder (1984). Olivine crystals with no MIs are assigned to “G1”, then the MI typologies are coded, e.g. starting with homogeneous glassy MI assigned to "G2", MI with bubbles to “G3”, and MI with bubbles and oxides to “G4”. The “G2” group is particularly variable in the Pucón products and reaches the highest percentages in the P2 sequence (>35%). The percentage of olivine crystals with preserved “primary MIs” (G2+G3+G4) also follows a certain order in term of the amount of olivine crystals in each volcanic deposit (considering that all the MI typologies are subject to PEC; e.g. Rose-Koga et al., 2021); from Pucón Ignimbrite, Chaimilla to the March 2015 eruption, the amount of olivine crystals with primary MIs (G2+G3+G4) decreases, and the percentage of olivine crystals with vapor bubbles (G3+G4) also decreases.

Olivine Mg# are listed in Appendix E. At the central eruptive vent of Villarrica, the Pucón olivine crystals are Mg-rich ($Fo_{76–88}$), and those from the 2015 eruption have the lowest Fo content (Fo_{76}), although fewer samples were analyzed, which could introduce a sampling bias. The Chaimilla olivine crystals are heterogeneous in composition ($Fo_{76–85}$, Fo_{80}±3%). The MECs show slightly less Mg-rich olivine crystals compared to Villarrica ($Fo_{73–86}$). Los Nevados olivine crystals are heterogeneous in composition ($Fo_{75–85}$, Fo_{80}±3%), Chaillupén has olivine crystals with high Mg# ($Fo_{84–86}$, Fo_{84}±1%), and lastly the Caburgua olivine crystals have heterogeneous Mg# ($Fo_{73–84}$, Fo_{80}±4%).

3.4 Major element content from glass inclusions

All original MI compositions were corrected by adjusting the K_D of the olivine melt and comparing with bulk rock compositions for the FeO_T/MgO ratio (Fig. 2; Appendix A) (Wallace et al., 2021). To correct for Fe-loss, we used Petrolog3 software (Danyushevsky LV, Plechov P. 2011), in addition to adjusting the iron content at equilibrium with the bulk rock MgO. We also considered the Fe^{2+}/Fe^{3+} analyses with the best-fit FeOT/MgO regression line (see also Robidoux et al., 2021).

The MIs from the Pucón ignimbrite were classified as basaltic to basaltic andesites and a few andesites were observed (SiO_2 = 47.3–62.8 wt.% and K_2O=0.19–1.60 wt.%); data plot in the field from calc-alkaline (CA) to high potassium calc-alkaline (HKCA) rocks (Fig. 2). The Chaimilla series is slightly richer in K_2O (0.20–1.67 wt.%), and olivine-hosted MIs were mostly classified as basaltic andesites, whereas MIs from the 2015 eruption were basaltic-andesites, with lower K_2O contents (0.78–0.91 wt.%).

The total MIs reported by Robidoux et al. (2021), regardless of the specific eruptive center (Gr. 1, 2), were more differentiated in the Los Nevados MEC (47.6–58.0 wt.% SiO_2; 0.27–1.21 wt.% K_2O), with Chaillupén ballistics representing the most felsic MIs (57.1–59.0 wt.%; 0.93–1.35 wt.% K_2O). Caburgua represents intermediate differentiated MIs (51.1–59.3 wt.% SiO_2), but the alkaline content is highest in these samples (0.62–1.78 wt.% K_2O).

3.5 MI description and MI volatile concentrations

A description of the MIs is given in Appendix D (following the classification of Robidoux et al., 2018). The water and carbon dioxide contents of the MIs are reported (mFTIR in Appendix F, SIMS in Appendix G, reproductibility test in Appendix H). Of the 167 samples analyzed by mFTIR, 37 were measured by SIMS with no loss or damage during transfer to an indium mount (Appendix H). The % difference in water concentration between mFTIR and SIMS averages 0.5% and 89 ppm for CO_2 content.

Of all the volatile analyses from the central eruptive vent of Villarrica (Table 1, Appendix F-G), the Pucón ignimbrite series records the highest volatile contents in terms of the respective H_2O-CO_2 pair (0.1–6.0 wt%; 9–1485 ppm), followed by the Chaimilla series (0.2–2.4 wt.%; 16–337 ppm; similar to Pioli et al., 2015) and the 2015 eruption (0.1–0.8 wt.%; 160–307 ppm). In the MECs, similarly high values are found for the Los Nevados series (0.1–3.4 wt%; 30–1568 ppm; see also Robidoux et al., 2021), but also lower values in the Chaillupén series (0.3–3.6 wt%; 29–329 ppm), and again in the Caburgua series (0.6–2.8 wt%; 139–677 ppm).

The S, Cl and F concentrations at the Villarrica center (Pucón ignimbrite, Chaimilla and 2015 eruptions) are highly variable (Appendix I) with the following ranges 103–2055 ppm, 11–1330 ppm and, 81–1556 ppm, respectively. The contents of S, Cl, F from MEC samples have the following ranges: 41–2581 ppm, 13–2356 ppm and 59–2473 ppm (anomalous spot >4000 ppm F content susceptible to represent mineral inclusion that contain solid fluorine phase), respectively.

3.6 Raman-corrected CO_2 contents

Twenty-five MI with shrinkage bubble (1.3–10.1 vol.%) were analyzed by Raman micro-spectroscopy for their CO_2 bubble contents to be calculated according to the presence of two intensity peaks at ~1285 and ~1380 cm^{-1} in the Raman spectrum, defined as Fermi diad peaks (Esposito et al., 2011; Frezzotti et al., 2012; Remigi et al., 2021). The Fermi diad spacing is proportional to the fluid density inside the bubble (see Appendix A), with results varying between 0.004 and 0.911 g/cm^3 in n = 25 shrinkage bubbles (Appendix J). The densimeter was chosen to accommodate larger range of Fermi diad space (102,65 – 105,47 cm^{-1}) that fit the polynomial equation from the previous author and accordingly to instrumental setting used in Robidoux et al. (2018). The derived (mass / glass density x volume) total CO_2 concentrations (in glass inclusions + bubbles) all range between 207–3336 ppm, according to our µRaman density results on the 25 shrinkage bubbles using the technique of Robidoux et al. (2018). In addition, n = 31 shrinkage bubbles were measured to correct the total CO_2 concentrations to 54–3529 ppm according to the model Mimic of Rasmussen et al. (2021) (Appendix I). These values exceed the original (uncorrected) shrinkage bubble equivalent glass inclusion CO_2 contents of 24–1413 ppm (Appendix I).

3.7 Noble gas isotopes in fluid inclusions

The analytical results of elemental and isotopic measurements of helium, neon and argon, together with other complementary information, are reported in Appendix K. The ^{4}He and ^{20}Ne concentrations measured in FIs from olivine crystals of scoria and ash samples varied from 2.8 × 10^{-14} to 1.6 × 10^{-13} mol/g (Fig. 3) and from 1.7 × 10^{-15} to 1.7 × 10^{-14} mol/g, respectively. The $^{4}He/^{20}Ne$ ratio was 3.9–42.9, compared to the atmospheric $^{4}He/^{20}Ne$ of 0.318 from Porcelli et al. (2002). The concentrations of ^{40}Ar, ^{38}Ar, and ^{36}Ar ranged from 1.5 × 10^{-13} to 1.5 × 10^{-12} mol/g, from 8.9 × 10^{-17} to 8.8 × 10^{-16} mol/g and from 4.9 × 10^{-16} to 5.0 × 10^{-15} mol/g, respectively. The $^{40}Ar/^{36}Ar$ ratio varied in the range 300–336, whereas the theoretical ratio in the atmospheric is $^{40}Ar/^{36}Ar$~296 (Porcelli et al., 2002). Both $^{40}Ar/^{36}Ar$ and $^{4}He/^{20}Ne$ indicate that all the gases released by the FIs contain an atmospheric component mixed with the magmatic one. The concentrations of $^{40}Ar^*$ vary from 2.6 × 10^{-15} to 1.1 × 10^{-13} mol/g. The $^{4}He/^{40}Ar^*$ varies from 1.4 to 10.5, with the typical mantle ratio being considered to be in the range of 1–5 (Marty, 2012).

The $^{3}He/^{4}He$ ratios corrected for atmospheric contamination (expressed as Rc/Ra values) vary between 4.0 and 7.6 Ra (Appendix K; Fig. 3), with a bias with uncorrected $^{3}He/^{4}He$ ratios generally ≤0.2 Ra, except for the sample HCH-2AS that showed a bias of 0.4 Ra.

4. Discussion

4.1 The oldest magmatic batch preserves original magma volatile contents

At Villarrica, the Pucón ingimbrite is the oldest and best studied postglacial eruption, the least degassed endmember, but also contains the MIs least affected by parameters of post-entrapment crystallization effects (Appendix L). The precision and accuracy of the volatile contents produced consistent calibration curves using SIMS (Appendix M), and the reproducibility of mFTIR vs. SIMS gave comparable results (Appendix N), although the mFTIR technique is limited to larger MIs (>30 µm). The Villarrica and MEC samples were therefore selected for inclusion using both techniques.

At Villarrica, the Pucón ingimbrite contain the highest volatile contain in the MI collection. Despite the presence of vapor bubbles (except for two samples of Pucón and Gr. Los Nevados 1: TVPI5AB and HLN1A3D, respectively) and PEC glasses subject to volatile diffusion, the Pucón series contains the most primitive olivine crystals and MIs recording the highest volatile contents (Fig. 4; Appendices E; F-H). Chaimilla's MI volatile contents are systematically lower than those of the Pucón ignimbrite for similar major element chemistry and cogenetic parental melt differentiation (Figs. 2, 4; Appendix I) while MI volatile contents from the 2015 eruptions are even lower (increasing degassing effect during MI entrapment; Fig 4).

Degassing is not the only cause for volatile variation in our samples. In order to evaluate why the Pucón ignimbrite magma represents the least degassed mafic explosive event and highest saturation pressures (Fig. 5a), we examined a series of geochemical parameters for the olivine crystals and grain size distributions of the respective volcanic deposits sampled in this study. There are two main points favoring the preservation of pre-eruptive volatile contents in the Pucón MI series; (i) high juvenile clast cooling rates, and (ii) high natural inclusion quenching rates. Firstly, since the smaller clast size favors a high cooling rate (Loyd et al., 2013), we infer that decreasing cooling rates may explain the variation in PEC-related artefacts observed in MI populations from successive Chaimilla and MEC eruptive sequences. Regardless of the eruptive center, the presence of juvenile clasts with a low degree of crystallinity is likely to indicate high magma cooling rates (e.g. Los Nevados, Robidoux et al., 2021). Previously, the larger clast sizes had been identified as the most crystalline (Robidoux et al., 2021), but their water contents are the lowest in our collection of MIs (Fig. 5c). The inverse correlation of grain size with MI water content in the same batch of olivine crystals (Fig. 5b, d) may be explained by an increase in H^+ diffusion which affects all of the pyroclasts (Fig. 5b-c). Secondly, we infer that low MI-trapping temperatures favor H^+ diffusion because of MIs with low water contents (Fig. 5bcd). This effect is explicitly related to low quenching rates which affect the solidification of MIs and accentuate the water diffusion into the olivine host (Fig. 5; Appendix L) (e.g. Massare et al., 2002; Gaetani et al., 2012). The estimated silicate glass transition temperature (Giordano et al., 2008), as well as the trapping MI temperatures (Putirka et al., 2008), in our data set correspond to the highest water contents measured in the MIs (Fig. 5d). Consequently, we would expect high MI quenching rates to prevent H^+ diffusion in samples from the Pucón ignimbrite.

4.2 Post-glacial magma degassing and chronological volatile saturation depth below Villarrica

There is a temporal transition in the pre-eruptive minimum saturation pressure conditions of eruptive centres at Villarrica between paroxysmal inner crater eruptions (C3) and clustered flank MECs in the primitive Villarrica caldera (C1-2) (Moreno and Clavero, 2006). We characterize the variation in saturation depth conditions of magmas that erupted at volcanic centers around Villarrica (Appendix A). The volatile contents and major element composition of the MIs are integrated into the solubility model from Iacono

Marziano and Whitam (2012) (Figs. 4, 6; Appendix A). Despite H_2O-CO_2 pairs being the focus of this study, the sulfur and halogen (Cl, F) contents remained constant from the start to finish of the Pucón eruption, as well as the subsequent paroxysmal explosions at Villarrica crater (Fig. 4; Appendix A, I).

The Pucón ignimbrite 3,510–3,710 yr B.P. (Silva et al., 2010) records the highest volatile content preserved in MI-hosted olivines among the entire studied volcanic deposits. Consequently, the Pucón ignimbrite potentially represent the deepest degassing processes inducing mafic magma ascent from below Villarrica, but also the oldest magma recharge event (<17.0 km; this study). The major subdivisions in the Pucón sequence of "Pb" and "P1 to P3" (Silva et al., 2010) represent individually different equilibrium pressure ranges (Appendix A), suggesting a polybaric system that may have transported several masses of ascending magmas. Among these subsequent batches of Pucón magmas, when the first magma batch reached the surface, the "Pb" opening sequence, it consisted of hot, volatile-saturated melts (1070–1140 °C) with saturation occurring between 2.5–7.9±0.63 km (1SD). This phase has been described as evolving from a strombolian to a more explosive Plinian eruptive style (Moreno and Clavero, 2006), and our new dataset shows that it was relatively water-rich (<3.6 wt%) and CO_2-rich (1485 ppm) (16.6±5.9 km, 1SD) (Figs. 4, 5). This study shows that the last Pucón event (P3) finally recorded ~>1200 ppm CO_2 and a maximum water content of 6.0 wt.%, which is higher than the 4.65 wt.% water content estimated with the thermobarometric model by Boschetty et al. (2020) (Figs. 4, 5, 6).

The Chaimilla fall deposit 3,180±40 yr B.P. (Costantini et al., 2011) is a key explosive eruptive event that occurred when the crater formed after the collapse of the edifice following the eruption of the Pucón ignimbrite (e.g. "C3" in Moreno and Clavero, 2006). On account of the very thin stratigraphic separation between the Pucón and the Chaimilla subsequent deposit (this study; Pioli et al., 2015), our new MI dataset demonstrate that the Chaimilla mafic magma represents a degassed, cooler (<1018–1134 °C) endmember of the Pucón ignimbrite (ibid. for S; Cl, F contents; Appendix A); it records lower pressure ranges (0.4–0.9 kb corresponding to the volatile-rich type 2 magma defined by Pioli et al., (2015) (Fo_{81-85} at 1.2 kb). This explosive paroxysm was saturated in volatiles for minimum depths of between 3.24 to 1.68±0.6 km. To illustrate the model for present-day conditions of mafic magma below Villarrica central crater, our new MI dataset indicates volatile saturation to at least 1.7 km in depth (Fig. 6), considering lithospheric depths of 3.1 ±0.6 km for CO_2-corrected MIs (±8.3kb). The crystallization equilibrium during the 2015 Strombolian paroxysm was ≤ 5.3 km (ca. 1110 °C) (Romero et al., 2022).

Given the solubility model results of magmas that persist below the present-day central crater (Appendix A; Figs. 4, 5, 6), the volatiles reach saturation conditions at >14.2–16.6 km while the magma starts crystallizing olivine at a depth of 19–35 km

(Morgado et al., 2015). This saturation depth range depth range partially matches the ~8–20 km zone of low resistivity detected by by magnetotelluric analysis which could be related to a region that favor melt transport below Villarrica (Pavez et al., 2023). Although the chronological evolution of magmatism at Villarrica may illustrate a TCMS model that persists into the present (Cashman et al., 2017; Boschetty et al., 2022). The Pucón ignimbrite provides petrological evidence for an early mantle-rooted magma that may transport derived melt at shallower depths. Although similar in composition (section 4.3), the subsequent Chaimilla event is a shallow (1.7–3.2 km) degassed residual melt, produced in similar conditions to the current feeder system (Fig. 6) (Blundy and Cashman, 2008).

4.3 Villarrica Caldera: volatile saturation depth and magma composition

Based on our new collection of bulk rock compositions and the dataset from the literature, we propose that Villarrica is a polygenetic system which has the potential to link its deeper central magmatic system to similar depth chambers beneath lateral MECs (Smith and Németh, 2017). The volatile content and degassing conditions reviewed in previous sections suggest a common mantle-derived volatile source, but entrapment pressure of MI that record the same order of lithostatic depths (≤ 21.3 km). On the other hand, compositional heterogeneities of the transported magmas are reported from bulk rock as MI chemistry between the center and the outer region of Villarrica (Fig. 5, 6).

Within the primary Villarrica Caldera 1 structure there are minor lateral eruptive fields, such as the Los Nevados cones (<2,600 yr B.P.), which also tapped deep magmatic batches (9.2 km; Robidoux et al., 2021) (Fig. 6). Our new MI-CO_2 content correction gives minimum saturation pressure values of up to 14.2–21.3 km. In comparison, Chaillupén MEC cones have saturated volatiles below <1.9 kb, (Avg. °T= 1169±8°C), which results in a lithostatic depth of < 0.3–6.8 km for melts erupting on the flanks of Villarrica. In contrast, the regional Caburgua (CHSEC) eruption has magmas that crystallized at 32–44 km (1163 °C) according to the model of Morgado et al. (2015). Based on our new CO_2 density-µRaman corrections (3.7–4.8 kb), we argue that the regional monogenetic cone of Caburgua could dissolve volatiles down to ~13.5–17.3 km, despite travelling up through a lithological basement far from the main stratovolcano.

The basement characteristics involve compositional heterogeneities of the transported magmas in the region of Villarrica according to our new bulk rock composition results (Fig. 7). Since the post-Licán Ingimbrite ~13.5 ky volcanic event (formation of Caldera 1 at Villarrica), the MEC and Villarrica datasets from previous authors demonstrate progressive sedimentary slab assimilation and/or crustal contamination/assimilation (Sr/Y, K_2O content), with a particularly strong evolution towards sediment-metasediment chemical end members with a “slab fluid” signature (Th/La, Sr/Nd, La/Sm, Th/Nb ratios; Fig. 7). This signature is present at Villarrica Los Nevados Gr.1 (HLN1), initial Pucón (Pb) and early Chaimilla deposits, but diminishes through space at distant MEC and monogenetic MEC Caburgua (Fig. 7; see spatial "slab fluid" vector graphically connecting our sample series from low to strong "slab fluid" signature). Diagnostic plots of Th/La vs. La/Ta show that the mantle wedge source of the magma was metasomatised by slab-derived 'supercritical' fluids in the water-rock system (Ferrando et al., 2019), which is graphically explained by the parallel axis vector (Fig. 7b). The exception in our sample set is the granitic lithic contaminated scoria, which could alternatively be explained by enrichment by hydrous silicate melts (Fig. 7b) and/or crustal assimilation (Fig. 7a, c-d). The “slab fluid” signature (Fig. 7d) also diminishes through time toward the intermediate to final eruptive phases (Los Nevados Gr.2 HLN2, Pucón P2-3, Chaimilla, Chaillupén) (Fig. 7). Spatial dissipation of the geochemical signature exists in other polygenetic-related MECs worldwide, for example, between the peripheral cone of Cono Navidad and the Lonquimay stratovolcano, Chile (Gilbert et al., 2014): The most striking difference is observed in MECs from the monogenetic Chichinautzin volcanic field and Popocatepetl, Mexico, where the slab signature decreases away from the stratovolcano (Robidoux et al., 2020). Away from the Villarrica C1-C3 caldera boundaries, this study clearly supports the idea that the regional Caburgua (CHSEC) monogenetic system is representative of how different mantle-crustal conditions affect magma transport, but more importantly, that potential mantle composition heterogeneities exist along the volcanic arc segment in the SVZ (Morgado et al., 2015; Hickey-Vargas et al., 2016; McGee et al., 2017).

4.4 Evidence of atmospheric and crustal-derived components in magmatic fluids

Volatiles are cycled between the atmosphere and the Earth's interior at subduction zones (Zellmer et al., 2015). In this geodynamic setting, slab dehydration at depths of several kilometers can differentially influence the composition of magmatic fluids generated in the overlying wedge. Subduction-related fluids are known to contain higher proportions of atmospheric components than intraplate and mid-oceanic ridge environments (Burnard et al., 1997). According to Hilton et al. (2002) and Sano and Fischer (2013), noble gases found in arc magmatic/hydrothermal fluids and trapped as fluid inclusions (FIs) in minerals are important indicators of the relative contributions of the subducted slab, crust and mantle to the fluids emitted by arc volcanoes. A recent compilation of light noble gases in the South American arc revealed that the average $^{40}Ar/^{36}Ar$ signature of all gas-rocks samples is ~339 (Lages et al., 2021b), which is well below that of MORB (~44,000; Moreira et al., 1998) and close to the atmospheric signature (~296; Porcelli et al., 2002). In rocks from Villarica (our samples and ones from Lages et al., 2021b), the observed $^{40}Ar/^{36}Ar$ ratios in FI range from 300 to 336, supporting the low isotopic signature already found along the South American Arc. Similar inferences can be made from the $^{4}He/^{20}Ne$ range (3.9–50.8), which is not far from the atmospheric ratio (0.318).

These atmospheric Ar-Ne isotopic signatures suggest significant contamination by an atmospheric component, consistent with their comparatively high abundances in air (compared to helium) (Hilton et al., 2002). Although contamination of surface rocks on exposure is possible, though difficult to confirm or exclude, recycling of atmospheric Ar into the mantle by dehydration of subducting oceanic crust has been suggested in several contexts (Matsumoto et al., 2001; Hopp and Ionov, 2011; Di Piazza et al., 2015; Rizzo et al., 2016, 2022; Robidoux et al., 2017, 2020; Battaglia et al., 2018; Lages et al., 2021a, 2021b). At Villarica volcano, the intricate plumbing system and the fact that it formed in a continental crust at about 45 km in depth must also be taken into account (Hickey-Vargas et al., 2016). Considering that the presence of an atmospheric component is a common feature of many volcanoes in the South American volcanic arc, and that most of these volcanoes were built above a continental crust several tens of kilometers in thickness, we can conclude that the atmospheric component in magmatic fluids from Villarica, and probably also other South American volcanoes, is either recycled into the mantle wedge from the subducting slab and/or acquired during magma ponding within the continental crust.

To investigate the role of the subducting slab and continental crust on the composition of the degassed magmatic fluids at Villarica, $^{3}He/^{4}He$ can be used as a useful tracer, coupled with petrological and geodynamic evidence (Fig. 8; Appendix K). In a global review of arc volcanism, Hilton et al. (2002) reported that: i) the highest $^{3}He/^{4}He$ ratios are in the MORB range (i.e. 8 ± 1Ra; Graham, 2002); ii) in many arc segments (including central and northern Chile, Peru and Ecuador) the highest $^{3}He/^{4}He$ ratio is below the MORB range (i.e. below 7 Ra); iii) the mean $^{3}He/^{4}He$ ratio of all arc segments is 5.4 ± 1.9 Ra. Recent studies in the Central and South American Volcanic Arcs have provided new measurements of helium isotopes in Fis hosted in olivine and pyroxene crystals, adding to our knowledge of $^{3}He/^{4}He$ variability in arc volcanoes (Lages et al., 2021a, 2021b; Rizzo et al., 2022 and references therein). The main results of this recent work are that: i) the mantle $^{3}He/^{4}He$ signature of the Central and South American Volcanic Arcs are within the MORB range, with the highest values measured in Guatemala (9 Ra, Pacaya volcano) and Colombia (8.8 Ra, Galeras volcano; Fig. 3b); ii) $^{3}He/^{4}He$ values below the MORB range are indicative of variable crustal contamination, often with an inverse relationship between Rc/Ra values and crustal thickness (this feature is mainly observed in the South American Volcanic Arc); iii) there is a progressive decrease in mantle wedge $^{3}He/^{4}He$ values, within the MORB range, coupled with variations in some key trace element ratios (i.e. Ba/La, Th/La, U/Th), resulting from a higher presence of subducted slab sediment fluids (rich in U and Th, from which radiogenic He is produced). This has been observed particularly in the Central American Volcanic Arc and the SVZ.

At Villarica volcano, Lages et al. (2021b) reported $^3He/^4He$ values as high as 6.7 Ra, which were interpreted as resulting from crustal contamination, although Plank (2005) pointed out that significant quantities of sediment-derived fluids are transferred to arc magmas in northern and southern Chile. In this work, we present new data on $^3He/^4He$ in FIs that mostly reflect the measurements presented by Lages et al. (2021b), except for one sample from Pucón that has a value of 7.6 Ra. This value is almost 1 Ra unit higher than the average values for Villarica volcano, suggesting that the continental crust effectively plays a role in lowering the $^3He/^4He$ values of pristine mantle fluids. A helium isotopic signature of 7.6 Ra is still lower than that expected for mantle values. However, in the light of the slab sediment fluid contribution suggested by Plank (2005) for this region of the SVZ and the relation between Rc/Ra and Th/La ratios of Lages et al. (2021b) (Fig. 9ab), we argue that the $^3He/^4He$ signature below Villarica is confirmed to be within the MORB range and that the complex plumbing system of the volcano plays an important role in lowering the mantle $^3He/^4He$. More work is required to investigate the variation in radiogenic ^4He (bulk mol/g content) in olivine FIs for the most well-studied polygenetic Villarrica basaltic andesites produced since the postglacial period.

Regardless of the primitive nature of the olivine (olivine Fo% or MI Mg# show no correlation with our Rc/Ra ratios; Fig. 3, 8), we suggest that the magmatic ^3He content decrease with crustal contamination and when wall rock interaction is more likely to slow down cooling magma reservoirs. This latter conclusion is already supported petrologically by major element MI trends (Fig. 2), bulk rock REE (Figs. 7) and noble gas isotopes (Figs. 3, 8), but could depend on cooling rates and chamber timescales (e.g. U-TH-He isotopic systematic; Kuritani et al., 2007; McGee et al., 2018). In addition, figure 9 details peripheral contamination effect as a potential source of recycled ^4He increase, which also occurs for bulk rock compositions indicating crustal interaction, such as Sr/Y ratios (> 20), and K_2O (wt%) content (Fig. 9cd). This correlation is not systematic for the Th/La ratio, used as an indicator of slab sediment fluid contribution (Fig 7b). This geochemical anomaly is only found for the Pucón recharge event (Th/La >0.2) during the post-glacial period of Villarrica and is absent from the Chaimilla-derived magma and other MEC eruptions (Fig. 9ab; Th/La < 0.2). Thus, ^4He contamination is weaker during Plinian events with high VEI explosive paroxysms (Pucón, Chaimilla). Our olivine FI dataset records the lowest ^4He content (g/mol) during the climax eruptive phase (Fig. 9). Such geochemical parameters indicate that less peripheral contamination is expected in basaltic andesites from parental magma (Pucón) that feed the main explosive paroxysms of Villarrica.

5. Conclusions

For the first time a joint comparison has been made based on melt volatiles, major and noble gases for a polygenetic volcanic system, that of Villarrica in the southern Andes. This study includes new detailed data on volatile saturation depths, with improved analyses for P-T-fO_2 pre-eruptive magma conditions based on new geobarometry calculations, and a solubility model that uses novel µRaman dataset to predict the original CO_2 contents in MIs with shrinkage bubbles. Two major petrogenetical problems were explored within this research providing of the following conclusions:

Temporally since the current 2 km-wide caldera formation (post glacial period, see Villarrica Unit 3, <~ 3.7 Kyr AP; Moreno and Clavero, 2006), the Villarrica stratovolcano forms a polygenetic system in which the magmatic volatile content decreases from the Pucón event (3.7 ky) to the March 2015 paroxysm. The parental mafic magma of the Pucón eruption might represents the pre-eruptive conditions of the Chaimilla event (<~ 2.6 Kyr AP (Pioli et al., 2015), but subsequent explosive eruptions record increasing degassing conditions below minimum saturation pressure depth equivalent (<~ 17.0 km). Mafic magma continued to evolve vertically from shallow storage depths to present conditions (<1.7–4.4 km), as well as laterally to nearby MECs (Chaillupén, Los Nevados) from post-glacial times. According to the noble gas study, the magmatic fluid signature varies with continental contamination during vertical transport of the mafic magmas; the isotopic noble gas MORB signature is richer in radiogenic ^{4}He at the MECs and smaller VEI eruptions (2015) (<6.7), while the high VEI explosive paroxysms of Villarrica (Pucón, Chaimilla) peak at Ra~7.6 (closer to the homogeneous mantle signature along the South American arc of 8–9 Ra; Lages et al., 2021).

Spatially the contrasting background geology (Caburgua) and divergent magmatic chemical source at 25 km from Caldera 1 confirm that the plumbing system architecture is complex and distinct between Villarrica itself and the flank MECs. The noble gas studies combined with bulk rock datasets for Villarrica (Pucón ignimbrite, Chaimilla, 2015 eruptive sequence) and flank eruptive centers (Grupo Los Nevados and Chaillupén and the closest regional MECs at Caburga) confirm a unique ascent and degassing behavior for each successive batch of mafic magma, due to different degrees of interaction with the crust for each one. All basaltic andesitic Villarrica magmas could be derived from a similar parental end member rooted in the asthenospheric mantle, but their typical slab fluid signature and crustal contamination effect, as evidenced by bulk rock chemistry, are variable in the central Villarrica vent and lateral MECs (see Morgado et al., McGee et al., 2017). The new noble gas dataset finally completes the scenario of spatial magma heterogeneities, confirming that the crustal effect of radiogenic ^{4}He lowers the original ^{3}He/^{4}He ratio as magma batches pond in the different zones below the Villarrica central crater and its flank MECs plumbing system.

Acknowledgements

This work is part of ANID, Fondecyt Iniciacion No 11190846 project of Philippe Robidoux (2019–2022). We are grateful to Dra Manuela Nazzari and Dir. Piergiorgio Scarlato for providing access to electron microprobe EMPA at Istituto Nazionale di Geofisica e Vulcanologia Sezione di Roma 1, HP-HT Lab. of Experimental Volcanology and Geophysic. The measurements were also supported by Elisabetta Del Bello and Alessio Pontiselli (INGV-Roma) through participation at the TransNational Access (TNA) in the framework of the EXCITE (Horizon 2020) research infrastructure. Special thanks are sent for Dr. Andrea Rizzo and staff from INGV-Palermo for analysis on noble gases; Mariano Tantillo and Mariagrazia Misseri helped mineral preparation with their assistance during noble gases isotope analysis. Special thanks are also addressed to Dra. Simona Ferrando from University of Torino for Raman studies. We address special acknowledgements for Universidad Mayor, Escuela de Geología as Universidad de Chile (Depart. Geología) Bsc. students Gloria Díaz, Aaron Sancho, Daniela Pasten and Prof. Clavero for active participation in the 2017–2022 field trips. ER-K, YM and PR deeply thank Nordine Bouden and Johan Villeneuve for their flawless support with the SIMS measurements and for the access to the Nancy preparation lab.

CAPTIONS

Table Captions:

Table 1 – Volcanic deposit characteristics. Sieved and non-sieved volcanic deposits are given geographical coordinates for outcrop location and additional material description. The granulometry is in Phi (φ) size. Fragment size and typology distribution (% per 100 randomly selected clasts) are classified strictly on Fisher (1966) classification in addition to the full spectrum of clastic material typology, classified according to White & Houghton (2006).

Table 2 – Volcanic event references for analysis

Figure Captions

Figure 1 – Location of study area. a) Map of the subduction zone, including arc segments from the Central Volcanic Zone (CVZ). White lines are inferred tectonic plate boundaries and arrow indicates direction of subduction. Colored dots are sampled spring sites with Rc values marked using quartile color code. All eruptive centers listed in the Smithsonian Global Volcanism Program's Holocene Volcano List (small black triangles). From north to south, oceanic plate segments with fracture zone abbreviations ending in "FZ" are linked to Juan Fernandez Ridge; Mocha FZ, Valdivia FZ, Chiloe FZ, and Chile Rise FZ. b) Stratigraphic extent of Villarrica Pucón ignimbrite for Units P1, P2 and initial Base Surge Deposit "Pb" (Moreno and Clavero, 2006) as delimited by Silva et al. (2010). The Caldera 1,2 and 3 boundaries (Moreno and Clavero, 2006) are marked, as well as extent of for Chaillupén and Los Nevados Groups (modified from same source; Robidoux et al., 2021), with Caburgua MECs restricted to Caburgua cone #1 sector for lava and pyroclastic deposits (modified from Moreno and Clavero, 2006; Morgado et al., 2015). The Chaimilla fallout deposit (Costantini et al., 2011) and Pucón (Silva et al., 2010) are shown with maximum covered areas from isopach ellipsoid.

Figure 2 – Major element compositions. The post entrapment-corrected MIs with their major element contents as a function of SiO_2 wt.% (see corrected dataset in Appendix I). The bulk rock analyses are shown by colored squares for each series. Dashed arrows indicate the approximate trend for groundmass crystallization of plagioclase (Pgl In) ± clinopyroxene (Px In). The trapped melts (MIs) evolve via a parental melt differentiation path (red arrow) or post-entrapment crystallization effects (PEC) (orange arrow). The post-entrapment crystallization effects are interpreted in Appendix L. The bulk rock composition of the 1971 Villarrica eruption is represented by grey dots and Caburgua-Huellemolle by a dark grey box (Hickey-Vargas et al., 2002; Morgado et al., 2015).a) K_2O vs SiO_2 classification for the volcanic series, b) CaO wt.%, c) Al_2O_3 wt.% where plagioclase (Pgl-In) is interpreted as residual melt plagioclase crystallization occurring before/during MI entrapment, d) Na_2O wt.% where the dark arrow represents the general tendency toward cogenetic differentiation in all our MI collection, e) MgO wt.%, f) FeO_T wt.%.

Figure 3 – The FI helium dataset. $^3He/^4He$ (R/Ra) ratio vs He concentration (mol/g) collected from analytical data of bulk fluid inclusions (FIs) hosted in olivine (Appendix K). Data from Rizzo et al. (2022) and Lages et al. (2021ab) represent the literature FI data, while our dataset of FIs in olivine crystals is represented by colored symbols (see legend in Figure 2). Samples 2015_B* (Villarrica 2015), HCH2A1* and HCH2A4C* (Chaillupén) are from Lages et al. (2021b) (Appendix K). Data are grouped as combined segments from Central American Volcanic Arc (CAVA; green/black colored symbols) and South American Volcanic Arc (South American VZ; yellow symbols). b) $^3He/^4He$ (R/R_A) vs He/Ne data ($^4He/^{20}Ne$) in FIs and free gases. Binary mixing (air-magmatic endmember) curves are from Lages et al. (2020, 2021) and calculated using maximum R_C/R_A values for each segment; grey delimits the MORB range (8±1 R_A). The free gas

results are classified according to Lages et al. (2021); Free gases of temperature > 100 °C; Free gases 50–100°C; Free gases < 50 °C.

Figure 4 – Volatile contents from melt inclusions at Villarrica. The solubility model is used for PEC-treated MIs only, applying the Iacono-Marziano et al. (2012) model to calculate isobars and degassing curves. a) CO_2 vs H_2O concentrations in melt inclusions from Villarrica. b) CO_2 vs H_2O concentrations in melt inclusions from MECs, c) Raman-corrected degassing paths (closed system degassing). The µRaman density represents all MIs treated with the method of Robidoux et al. (2018) using our CO_2 density dataset measured by µRaman. The Mimic model is applied to all MIs with vapor bubbles producing new CO_2 content as output CO_2vbg (Rasmussen et al., 2020), which is the result of the calculated reconstruction of the total MI volume CO_2 content reconstruction using the vapor growth model of the same authors.

Figure 5 – Post entrapment crystallization saturation pressure and temperature conditions: chronological order. a) Saturation pressure (kb), of Villarrica center (red) and MECs (blue) for minimum saturation pressures. The µRaman CO_2-corrected MIs represent pressures with bubble symbols and vertical black arrow point connect non-corrected to CO_2-corrected contents. b) H_2O wt% content from MIs is represented by vertical bars for Villarrica center (red) and MECs (blue). H^+ diffusion is interpreted for increasing effect (upward arrow) or decreasing effect (downward arrow). c) Inaman's (1952) Md grain size parameter indicate increased negative values for larger pyroclast size. Explosive fragmentation is inferred to cause an increased production of large clast sizes at the sampled outcrop (upward arrow), while clast cooling rate decreases (downward arrow) as clast size increases. d) Temperature (°C), of Villarrica center (red) and MECs (blue). The thin vertical bars are minimum to maximum recorded PEC MIs for this study. The grey colored boxes represent minimum and maximum temperatures (°C) using Tg output obtained using the Mimic model (Rasmussen et al. 2020), which is the glass transition temperature (Giordano et al., 2008). The MI quenching rate (interpreted) subjectively decreases along the same series of olivine crystals (downward arrow).

Figure 6 – Villarrica depth cross section for solubility model. West to east Villarrica profile for magma crystallization conditions (lithostatic pressure gradient is 3.7 kb/km). Vertical scale X2 applies to framework below >2.0 km in depth and vertical scale X1 applies to framework between summit (2847 m.) and 2.0 km in depth. Horizontal distances are not to scale. Minimum saturation depths (km) are shown with an abbreviation code for each eruptive event based on the literature (Moreno and Clavero, 2006); same color code as for Figure 2, except for literature Chaimilla black letters abbreviated to "Ch*" are crystallization depths of ascending magmas from Pioli et al. (2015).The boxes with colored borders are minimum and maximum saturation pressures (Bar) recorded by MI solubility models and thin vertical bars are minimum and maximum ranges for µRaman CO_2 corrections applied in the present study. Arrow intervals stand for vertical interval depths in black characters for Magma reservoir* (Lohmar et al. 2008 and 2012; Delgado et al., 2017; Pavez et al., 2023), Paroxysm source* (2015) (Romero et al., 2022) and Low Resistivity Zone* (Pavez et al., 2023)

where partial melts develop. Villarrica olivine* (19–35 km) and CHSEC olivine (32–44 km) are from Morgado et al. (2015) and represent crystallization depths calculated using geothermobarometry. Background volcanism is modified from Moreno and Clavero (2006). The Rc/Ra dataset is from this study, except for the Villarrica paroxysm source and the duplicate Chaillupén sample (Lages et al., 2021b).

Figure 7 – Magma source evolution from bulk rock. Trace element and REE ratio trends from bulk rock analyses are compared with literature data. The volcanic arc bulk rocks are compositions for volcanic arc segments combining Central + South Volcanic Zone C-SVZ and North Volcanic Zone NVZ (database in Lages et al., 2021a, b) and CAVA (database in Rizzo et al., 2022) samples. The sediments sampled in the trench seawards of the Mocha FZ Fernandez Ridge MVFZ are all datasets from Lucassen et al. (2010) used to estimate the potential contribution of slab sediments. Volcanic eruption event abbreviations for bulk rock data in this study use the same names as in Moreno and Clavero (2006). The tendency for spatial enrichment and temporal decrease of slab fluid signature is illustrated in each figure with blue line toward black arrow. The primitive mantle PM is from Mc Donought et al., (1995). Our primitive starting member is represented by the Pb abbreviation for Pucón opening phase. a) Th/La vs. Sm/La, where OIB, MORB (Sun and McDonough, 1989) and sediment end members are data from Plank (2005), modified from McGee et al. (2017), modified Oceanic Crust value AOC from Jacques et al. (2014), b) Modified diagnostic Th/La vs. La/Ta diagram to distinguish the nature of natural as experimental slab-derived fluids for supercritical fluids and hydrous-silicate melts in the rock-fluid system released by different lithologies at high P-T conditions (Ferrando et al., 2019). Our dataset and the literature samples are filtered only for analyses having MgO > 4 wt%, LOI < 4 wt%, and Na_2O/K_2O < 8 to be plotted in order to consider the most primitive rocks.), c) Sr/Nd vs. La/Sm, where approximate tendency for addition of slab melt (sediment + AOC) to a depleted (BAM) mantle end member composition attributed to Villarrica model modified from Wieser et al. (2018). Our model identifies for crustal contamination and sediment addition, d) Sr/Th vs. Th/Ce, where arrows point to fluid and assimilation tendencies modified from McGee et al. (2017)'s modelling of end-member components using granitoid xenoliths, linked to samples from this study (Pucón P3 lithic fragments).

Figure 8 – $^3He/^4He$ for FIs corrected for atmospheric contamination (Rc/Ra) vs magmatic fluid tracers. a) Mean Th/La in subducting sediment columns (Plank, 2014) and volcanic arc trenches (bulk composition added in this paper for CVZ and Lages et al., 2021b; database filtered for < 58 wt% SiO_2). CAVA bulk composition from Rizzo et al., 2022. The same symbols are used as in previous figures for MIs, with the Pucón ignimbrite series Pb considered as the parental magmatic fluid and/or melt for the rest of the dataset produced in this study. B) The $^3He/^4He$ FIs corrected for atmospheric contamination (Rc/Ra) vs. $CO_2/^3He$ systematics for South American fluids calculated as mol/g from mass spectrometry; the crust-mantle binary mixing line (in blue) assumes an Ra of 7.9 (avg. SVZ taken from Lages et al., 2021b). All lines and "X" symbols are fumarole data taken from Lages et al. (2021ab) and CAVA data from Rizzo et al. (2022).

Figure 9 – The influence of geochemical parameters on trapping conditions of $^3He/^4He$ FIs: chronological order. The bulk rock collection is from the following authors: Hickey-Vargas, 1989; Lohmar, 2008; Costantini et al., 2011; Pioli et al., 2015; Morgado et al., 2015; Hickey-Vargas et al., 2016; McGee et al., 2017). a) Th/La slab sediment ratio used to test possible slab control on the $^3He/^4He$ signature of the mantle wedge along the Andes and Villarrica, b) ^4He content (g/mol) from this study, c) Sr/Y to detect peripheral contamination, from our bulk rock collection and the literature d) K_2O wt.% content from PEC melt inclusions, with minimum and maximum interval bars. The median value is arbitrary, representing the range of minimum and maximum K_2O wt.% contents in the dataset by eruptive event. The bulk rock K_2O wt.% contents are from this study and the literature.

Supplementary Material

(File)

Appendix A – Supplementary Material Methodology Review.

(Tables)

Appendix B – Table A.1: Full inclusion reference analysis.

Appendix C – Table A.2: Bulk-rock analysis of Villarrica samples.
Major element analysis based on ICPMS. LOI values were corrected for oxygen uptake in the conversion of FeO to Fe_2O_3T (wt.%) in the furnace. Ratios for each eruptive event were reported as FeO/Fe_2O_3. Trace elements and REE were analyzed by inductively coupled plasma mass spectrometry. Trace element ratios are calculated directly from the values in the table (weight ppm ratio) with no normalization to the standards in the literature.

Appendix D – Table A.3: Olivine populations statistics.
Classification of olivine series described for the presence of the following MI typologies (Robidoux et al., 2018): G1 (no inclusions), G2 glassy inclusions, G3 glassy inclusions+vapor bubble, G4 glassy inclusions+vapor bubble+spinel, G5 crystallized MIs, GR MI associated with boundary (reentrant or hourglass). Inclusion morphologies and dimensions are given in microns.

Appendix E – Table A.4: Electron microprobe analyses of original Villarrica and MEC olivine chemistry.

Appendix F – Table A.5: H_2O-CO_2 contents from FTIR.
a) H_2O (as OH^{-1}) at 3,550 cm^{-1} peak, b) CO_2 content as CO_3^{2-} double peak (1,435-1,515 cm^{-1}).

Appendix G – Table A.6: Volatile contents from SIMS.

Appendix H – Table A.7: mFTIR and SIMS reproducibility.
The selected mFTIR H_2O - CO_2 contents are compared to H_2O SIMS contents with error bars according to respective error sources. The wt. % error for [H_2O] with mFTIR assumes the sum of the following errors: (1) median absorbance (Abs.) graphical error between closest cm^{-1} records on IR spectrum to the left and right of the central peak position 3,550 cm^{-1}, (2) thickness deviation from the wafer (μm), (3) difference between replicate analysis "a" and "b". The STD error on eruption series from the density (g/cm^3) and absorption coefficients (mol^{-1} cm^{-1}) is only considered if EMPA results are not available. The wt. % error for [H_2O] with SIMS uses the %STD error from "^{16}O - ^{1}H" calibration curves. The wt. % error for [CO_3^{2-}] using mFTIR (ppm units) uses the same parameters as for [H_2O] (in wt.%), but graphical error depends on the double peak 1,435 – 1,515 cm^{-1}. The wt. % error for [CO_2] using SIMS (ppm units) uses the %STD error from "^{12}C" calibration curves.

Appendix I – Table A.8: Major element and volatile chemistry of Villarrica PEC glass inclusions.
Olivine compositions are given in Fo%, and geothermobarometer results for solubility models are calculated according to Iacono-Marziano et al. (2012). Conditions for Rasmussen method and Raman corrected volatile contents are given for saturation pressure models.

Appendix J – Table A.9: Raman CO_2 density and spectrum identification in shrinkage bubbles.

Appendix K – Table A.10: Noble gas isotopes.

Appendix L – Table A.11: Parameters of post entrapment crystallization effects.

Supplementary Material (Figures)

Appendix M – Figure A.1: Calibration of SIMS parameters for volatiles species.
The set of standards with known volatile contents are given for a) $^{12}C^-$, b) $^{13}C^-$, c) $^{16}OH^-$, d) $^{19}F^-$, e) $^{32}S^-$, f) $^{35}Cl^-$. A Cs^+ primary beam with a current of 1 nA and an electron gun is used to compensate for charge build-up at the sample surface. A 3-minute pre-sputter with a 30 × 30 μm square raster was applied, then analyses were performed on the 15 to 20 μm spot in the centre of the raster-cleaned area by a mechanical aperture placed at the secondary ion image plane. The resolving mass of ≈7000 (with the contrast aperture at 400 μm, the energy aperture at 40 eV, the entrance slit at 52 μm and the exit slit at 173 μm) meant that complete discrimination of mass interferences was achieved ($^{34}S^{1}H$ from ^{35}Cl, ^{17}O from $^{16}O^{1}H$, $^{29}Si^{1}H$ from ^{30}Si and $^{31}P^{1}H$

from ^{32}S). We collected signals for ^{12}C (8 seconds), ^{17}O (3 seconds), $^{16}O^{1}H$ (6 seconds), ^{18}O (3 seconds), ^{19}F (4 seconds), ^{27}Al (3 seconds), ^{30}Si (3 seconds), ^{32}S (4 seconds) and ^{35}Cl (6 seconds; counting times in brackets), with 2 seconds waiting time after each switch of the magnet. This cycle was repeated 10 times for each analysis. One measurement lasted 12 min per spot.

Appendix N – Figure A.2: mFTIR and SIMS reproductibility.

Volatile contents of MIs at Villarrica with H_2O concentrations in MIs from Villarrica. The mFTIR H_2O–CO_2 content is compared with the H_2O–CO_2 SIMS content with error bars. The MI samples containing shrinkage bubbles are represented by a circle with a black border. a) Comparison of the H_2O content is shown with error bars from Appendix C. The legend shows the four groups of quartiles used with grey-toned circles and each one represents the following categories in μm^3 unit volume (Vo) Q_1 (3,4E-09 – 8,0E-08); Q_2 (8,0E-08 – 2,5E-07); Q_3 (2,5E-07 – 5,4E-07); Q4 (5,4E-07b – 1,2E-05). b) Comparison of the CO_2 content is shown with error bars. Each eruption is color coded according to the legend.

References

1. Aiuppa, A., Bitetto, M., Francofonte, V., Velasquez, G., Parra, C.B., Giudice, G., Liuzzo, M., Moretti, R., Moussallam, Y., Peters, N. and Tamburello, G., (2017). A CO2-gas precursor to the March 2015 Villarrica volcano eruption. Geochemistry, Geophysics, Geosystems, 18(6), 2120-2132.
2. Battaglia, A., Bitetto, M., Aiuppa, A., Rizzo, A. L., Chigna, G., Watson, I. M., ... & de Moor, M. J. (2018). The Magmatic gas Signature of Pacaya Volcano, with implications for the volcanic CO2 flux from Guatemala. Geochemistry, Geophysics, Geosystems, 19(3), 667-692.
3. Blundy, J., & Cashman, K. (2008). Petrologic reconstruction of magmatic system variables and processes. Reviews in Mineralogy and Geochemistry, 69(1), 179-239.
4. Boschetty, F.O., Ferguson, D.J., Cortés, J.A., Morgado, E., Ebmeier, S.K., Morgan, D.J., Romero, J.E. and Silva Parejas, C., (2022). Insights into magma storage beneath a frequently erupting arc volcano (Villarrica, Chile) from unsupervised machine learning analysis of mineral compositions. Geochemistry, Geophysics, Geosystems, 23(4), e2022GC010333.
5. Boudoire, G., Rizzo, A. L., Arienzo, I., & Di Muro, A. (2020). Paroxysmal eruptions tracked by variations of helium isotopes: inferences from Piton de la Fournaise (La Réunion island). Scientific Reports, 10(1), 9809.
6. Brahm, R., Parada, M. A., Morgado, E., Contreras, C., & McGee, L. E. (2018). Origin of Holocene trachyte lavas of the Quetrupillán volcanic complex, Chile: Examples of residual melts in a rejuvenated crystalline mush reservoir. Journal of Volcanology and Geothermal Research, 357, 163-176.
7. Burnard, P., Graham, D., & Turner, G. (1997). Vesicle-specific noble gas analyses

of" popping rock": implications for primordial noble gases in Earth. Science, 276(5312), 568-571.

8. Cashman, K. V. (2004). Volatile controls on magma ascent and eruption. Washington DC American Geophysical Union Geophysical Monograph Series, 150, 109-124.
9. Cashman, K. V., Sparks, R. S. J., & Blundy, J. D. (2017). Vertically extensive and unstable magmatic systems: a unified view of igneous processes. Science, 355(6331), eaag3055.
10. Cassidy, M., Manga, M., Cashman, K., & Bachmann, O. (2018). Controls on explosive-effusive volcanic eruption styles. Nature communications, 9(1), 2839.
11. Costantini, L., Pioli, L., Bonadonna, C., Clavero, J., & Longchamp, C. (2011). A late Holocene explosive mafic eruption of Villarrica volcano, Southern Andes: The Chaimilla deposit. Journal of Volcanology and Geothermal Research, 200(3-4), 143-158.
12. Danyushevsky, L. V., Leslie, R. A., Crawford, A. J., & Durance, P. (2004). Melt inclusions in primitive olivine phenocrysts: the role of localized reaction processes in the origin of anomalous compositions. Journal of Petrology, 45(12), 2531-2553.
13. Danyushevsky, L. V., & Plechov, P. (2011). Petrolog3: Integrated software for modeling crystallization processes. Geochemistry, Geophysics, Geosystems, 12(7).
14. Delgado, F., Pritchard, M. E., Ebmeier, S., González, P., & Lara, L. (2017). Recent unrest (2002–2015) imaged by space geodesy at the highest risk Chilean volcanoes: Villarrica, Llaima, and Calbuco (Southern Andes). Journal of Volcanology and Geothermal Research, 344, 270-288.
15. De Maisonneuve, C. B., Dungan, M. A., Bachmann, O., & Burgisser, A. (2012). Insights into shallow magma storage and crystallization at Volcán Llaima (Andean southern volcanic zone, Chile). Journal of Volcanology and Geothermal Research, 211, 76-91.
16. DeMets, C. (2001). A new estimate for present-day Cocos-Caribbean plate motion: Implications for slip along the Central American volcanic arc. Geophysical research letters, 28(21), 4043-4046. https://doi.org/10.1029/2001GL013518
17. Di Piazza, A., Rizzo, A. L., Barberi, F., Carapezza, M. L., De Astis, G., Romano, C., & Sortino, F. (2015). Geochemistry of the mantle source and magma feeding system beneath Turrialba volcano, Costa Rica. Lithos, 232, 319-335.
18. Edmonds, M., Liu, E. J., & Cashman, K. V. (2022). Open-vent volcanoes fuelled by depth-integrated magma degassing. Bulletin of Volcanology, 84(3), 28.
19. Esposito, R., Bodnar, R.J., Danyushevsky, L.V., De Vivo, B., Fedele, L., Hunter, J., Lima, A. and Shimizu, N., (2011). Volatile evolution of magma associated with the Solchiaro eruption in the Phlegrean Volcanic District (Italy). Journal of Petrology, 52(12), 2431-2460.
20. Fall, A., Tattitch, B., & Bodnar, R. J. (2011). Combined microthermometric and Raman spectroscopic technique to determine the salinity of H2O–CO2–NaCl fluid inclusions based on clathrate melting. Geochimica et Cosmochimica Acta, 75(4), 951-964.
21. Ferrando, S., Petrelli, M., & Frezzotti, M. L. (2019). Gradual and selective

trace-element enrichment in slab-released fluids at sub-arc depths. Scientific Reports, 9(1), 16393.

22. Frezzotti, M. L., Tecce, F., & Casagli, A. (2012). Raman spectroscopy for fluid inclusion analysis. Journal of Geochemical Exploration, 112, 1-20.
23. Gaetani, G. A., O'Leary, J. A., Shimizu, N., Bucholz, C. E., & Newville, M. (2012). Rapid reequilibration of H2O and oxygen fugacity in olivine-hosted melt inclusions. Geology, 40(10), 915-918.
24. Geiger, H., Troll, V. R., Jolis, E. M., Deegan, F. M., Harris, C., Hilton, D. R., & Freda, C. (2018). Multi-level magma plumbing at Agung and Batur volcanoes increases risk of hazardous eruptions. Scientific Reports, 8(1), 10547.
25. Gherardi, F., Barsanti, M., Principe, C., & Magro, G. (2022). Helium isotopes in Plinian and inter-Plinian volcanic products of Vesuvius, Italy. Frontiers in Earth Science, 10, 1011203.
26. Gilbert, D., Freundt, A., Kutterolf, S., & Burkert, C. (2014). Post-glacial time series of explosive eruptions and associated changes in the magma plumbing system of Lonquimay volcano, south central Chile. International Journal of Earth Sciences, 103, 2043-2062.
27. Graham, D. W. (2002). Noble gas isotope geochemistry of mid-ocean ridge and ocean island basalts: Characterization of mantle source reservoirs. Reviews in mineralogy and geochemistry, 47(1), 247-317. https://doi.org/10.2138/rmg.2002.47.8
28. Heinrich, M., Cronin, S. J., Torres-Orozco, R., Colombier, M., Scheu, B., & Pardo, N. (2020). Micro-porous pyroclasts reflecting multi-vent basaltic-andesite Plinian eruptions at Mt. Tongariro, New Zealand. Journal of Volcanology and Geothermal Research, 401, 106936.
29. Hermann, J., & Rubatto, D. (2009). Accessory phase control on the trace element signature of sediment melts in subduction zones. Chemical Geology, 265(3-4), 512-526.
30. Hickey-Vargas, R., Sun, M., & Holbik, S. (2016). Geochemistry of basalts from small eruptive centers near Villarrica stratovolcano, Chile: evidence for lithospheric mantle components in continental arc magmas. Geochimica et Cosmochimica Acta, 185, 358-382.
31. Hickey-Vargas, R., Roa, H. M., Escobar, L. L., & Frey, F. A. (1989). Geochemical variations in Andean basaltic and silicic lavas from the Villarrica-Lanin volcanic chain (39.5 S): an evaluation of source heterogeneity, fractional crystallization and crustal assimilation. Contributions to Mineralogy and Petrology, 103, 361-386.
32. Hilton, D. R., Fischer, T. P., & Marty, B. (2002). Noble gases and volatile recycling at subduction zones. Reviews in mineralogy and geochemistry, 47(1), 319-370.
33. Hopp, J., & Ionov, D. A. (2011). Tracing partial melting and subduction-related metasomatism in the Kamchatkan mantle wedge using noble gas compositions. Earth and Planetary Science Letters, 302(1-2), 121-131.
34. Iacono-Marziano, G., Morizet, Y., Le Trong, E., & Gaillard, F. (2012). New experimental data and semi-empirical parameterization of H2O–CO2 solubility in mafic melts. Geochimica et Cosmochimica Acta, 97, 1-23.
35. Jacques, G., Hoernle, K., Gill, J., Wehrmann, H., Bindeman, I., & Lara, L. E. (2014). Geochemical variations in the Central Southern Volcanic Zone, Chile (38–43 S):

the role of fluids in generating arc magmas. Chemical Geology, 371, 27-45.
36. Jarrard, R. D. (1986). Relations among subduction parameters. Reviews of Geophysics, 24(2), 217-284.
37. Kessel, R., Schmidt, M. W., Ulmer, P., & Pettke, T. (2005). Trace element signature of subduction-zone fluids, melts and supercritical liquids at 120–180 km depth. Nature, 437(7059), 724-727.
38. Kuritani, T., Yokoyama, T., & Nakamura, E. (2007). Rates of thermal and chemical evolution of magmas in a cooling magma chamber: A chronological and theoretical study on basaltic and andesitic lavas from Rishiri Volcano, Japan. Journal of Petrology, 48(7), 1295-1319.
39. Lages, J., Rizzo, A.L., Aiuppa, A., Samaniego, P., Le Pennec, J.L., Ceballos, J.A., Narvaez, P.A., Moussallam, Y., Bani, P., Schipper, C.I. and Hidalgo, S., (2021a). Noble gas magmatic signature of the Andean Northern Volcanic Zone from fluid inclusions in minerals. Chemical Geology, 559, 119966. https://doi.org/10.1016/j.chemgeo.2020.119966
40. Lages, J., Rizzo, A. L., Aiuppa, A., Robidoux, P., Aguilar Contreras, R., Apaza Choquehuayta, F. E., & Masías Alvarez, P. J. (2021b). Crustal controls on light noble gas isotope variability along the Andean Volcanic Arc. uri: issn: 2410339X. https://doi.org/10.1016/j.chemgeo.2020.119966
41. Lehr, J., Bredemeyer, S., Rabbel, W., Thorwart, M., & Franco, L. (2022). Comparative interevent time statistics of degassing and seismic activity at Villarrica Volcano (Chile). Authorea. May 07, 2020.
42. Liu, E.J., Wood, K., Mason, E., Edmonds, M., Aiuppa, A., Giudice, G., Bitetto, M., Francofonte, V., Burrow, S., Richardson, T. and Watson, M., (2019). Dynamics of outgassing and plume transport revealed by proximal unmanned aerial system (UAS) measurements at Volcán Villarrica, Chile. Geochemistry, Geophysics, Geosystems, 20(2), 730-750.
43. Lloyd, A. S., Plank, T., Ruprecht, P., Hauri, E. H., & Rose, W. (2013). Volatile loss from melt inclusions in pyroclasts of differing sizes. Contributions to Mineralogy and Petrology, 165, 129-153.
44. Lohmar, S., Parada, M., Gutiérrez, F., Robin, C., & Gerbe, M. C. (2012). Mineralogical and numerical approaches to establish the pre-eruptive conditions of the mafic Licán Ignimbrite, Villarrica Volcano (Chilean Southern Andes). Journal of Volcanology and Geothermal Research, 235, 55-69.
45. Lohmar, S. (2008). Petrologia de las ignimbritas Lican y Pucon (Volcan Villarrica) y Curacautín (Volcan Llaima) en los Andes del sur de Chile.
46. Lucassen, F., Wiedicke, M., & Franz, G. (2010). Complete recycling of a magmatic arc: evidence from chemical and isotopic composition of Quaternary trench sediments in Chile (36–40 S). International Journal of Earth Sciences, 99, 687-701.
47. Marsh, B. D. (2015). Magma chambers. In The encyclopedia of volcanoes (pp. 185-201). Academic Press.
48. Marty, B. (2012). The origins and concentrations of water, carbon, nitrogen and noble gases on Earth. Earth and Planetary Science Letters, 313, 56-66.
49. Massare, D., Métrich, N., & Clocchiatti, R. (2002). High-temperature experiments on silicate melt inclusions in olivine at 1 atm: inference on temperatures of

homogenization and H2O concentrations. Chemical Geology, 183(1-4), 87-98.
50. Matsumoto, T., Chen, Y., & Matsuda, J. I. (2001). Concomitant occurrence of primordial and recycled noble gases in the Earth's mantle. Earth and Planetary Science Letters, 185(1-2), 35-47.
51. McGee, L.E., Brahm, R., Rowe, M.C., Handley, H.K., Morgado, E., Lara, L.E., Turner, M.B., Vinet, N., Parada, M.Á. and Valdivia, P., (2017). A geochemical approach to distinguishing competing tectono-magmatic processes preserved in small eruptive centres. Contributions to Mineralogy and Petrology, 172, 1-26.
52. McGee, L., Morgado, E., Brahm, R., Parada, M.Á., Vinet, N., Lara, L.E., Flores, A., Turner, M., Handley, H. and Nowell, G., (2019). Stratigraphically controlled sampling captures the onset of highly fluid-fluxed melting at San Jorge volcano, Southern Volcanic Zone, Chile. Contributions to Mineralogy and Petrology, 174, 1-24.
53. Mordensky, S. P., & Wallace, P. J. (2018). Magma storage below Cascades shield volcanoes as inferred from melt inclusion data: A comparison of long-lived and short-lived magma plumbing systems. Journal of Volcanology and Geothermal Research, 368, 1-12.
54. Moreira, M. A., & Kurz, M. D. (2013). Noble gases as tracers of mantle processes and magmatic degassing. The noble gases as geochemical tracers, 371-391.
55. Moreno, H., & Clavero, J. R. (2006). Geología del volcán Villarrica: Regiones de la Araucanía y de Los Lagos. Servicio Nacional de Geología y Minería, Subdirección Nacional de Geología.
56. Morgado, E., Parada, M. A., Contreras, C., Castruccio, A., Gutiérrez, F., & McGee, L. E. (2015). Contrasting records from mantle to surface of Holocene lavas of two nearby arc volcanic complexes: Caburgua-Huelemolle Small Eruptive Centers and Villarrica Volcano, Southern Chile. Journal of Volcanology and Geothermal Research, 306, 1-16.
57. Moussallam, Y., Lee, H.J., Ding, S., DeLessio, M., Everard, J.L., Spittle, E., Lu, G., Baur, J., Glazer, E., Peccia, A. and Zaman, M., (2023). Temperature of the Villarrica lava lake from 1963 to 2015 constrained by phase-equilibrium and a new glass geothermometer for Basaltic Andesites. Journal of Petrology, 64(2), egad003.
58. Moussallam, Y., Bani, P., Curtis, A., Barnie, T., Moussallam, M., Peters, N., Schipper, C.I., Aiuppa, A., Giudice, G., Amigo, Á. and Velasquez, G., (2016). Sustaining persistent lava lakes: Observations from high-resolution gas measurements at Villarrica volcano, Chile. Earth and Planetary Science Letters, 454, 237-247.
59. Nuccio, P. M., Paonita, A., Rizzo, A., & Rosciglione, A. (2008). Elemental and isotope covariation of noble gases in mineral phases from Etnean volcanics erupted during 2001–2005, and genetic relation with peripheral gas discharges. Earth and Planetary Science Letters, 272(3-4), 683-690.
60. Pavez, M., Brasse, H., Kapinos, G., Díaz, D., Lara, L. E., & Schill, E. (2023). Magma storage and transfer in the Villarrica volcanic chain, South Chile: MT insights into volcano-tectonic interactions. Journal of Volcanology and Geothermal Research, 439, 107832.
61. Plank, T., & Langmuir, C. H. (1998). The chemical composition of subducting

sediment and its consequences for the crust and mantle. Chemical geology, 145(3-4), 325-394.

62. Plank, T. (2005). Constraints from thorium/lanthanum on sediment recycling at subduction zones and the evolution of the continents. Journal of Petrology, 46(5), 921-944.
63. Pioli, L., Scalisi, L., Costantini, L., Di Muro, A., Bonadonna, C., & Clavero, J. (2015). Explosive style, magma degassing and evolution in the Chaimilla eruption, Villarrica volcano, Southern Andes. Bulletin of Volcanology, 77, 1-14.
64. Porcelli, D., Ballentine, C.J. and Wieler, R. (2002). An introduction to noble gas geochemistry and cosmochemistry. Rev. Min. Geoch. 47: 1-18.
65. Rasmussen, D. J., Plank, T. A., Wallace, P. J., Newcombe, M. E., & Lowenstern, J. B. (2020). Vapor-bubble growth in olivine-hosted melt inclusions. American Mineralogist, 105(12), 1898-1919.
66. Remigi, S., T. Mancini, S. Ferrando, M.-L. Frezzotti (2021). Interlaboratory Application of Raman CO_2 Densimeter Equations: Experimental Procedure and Statistical Analysis Using Bootstrapped Confidence Intervals. Applied Spectroscopy, 75(7), 867-881.
67. Rizzo, A. L., Robidoux, P., Aiuppa, A., & Di Piazza, A. (2022). $^3He/^4He$ Signature of Magmatic Fluids from Telica (Nicaragua) and Baru (Panama) Volcanoes, Central American Volcanic Arc. Applied Sciences, 12(9), 4241.
68. Rizzo, A.L., Pelorosso, B., Coltorti, M., Ntaflos, T., Bonadiman, C., Matusiak-Małek, M., Italiano, F. and Bergonzoni, G., (2018). Geochemistry of noble gases and CO_2 in fluid inclusions from lithospheric mantle beneath Wilcza Góra (Lower Silesia, southwest Poland). Frontiers in Earth Science, 6, 215
69. Robidoux, P., Aiuppa, A., Rotolo, S. G., Rizzo, A. L., Hauri, E. H., & Frezzotti, M. L. (2017). Volatile contents of mafic-to-intermediate magmas at San Cristóbal volcano in Nicaragua. Lithos, 272, 147-163.
70. Robidoux, P., Frezzotti, M. L., Hauri, E. H., & Aiuppa, A. (2018). Shrinkage bubbles: the C–O–H–S magmatic fluid system at San Cristóbal volcano. Journal of Petrology, 59(11), 2093-2122.
71. Robidoux, P., Roberge, J., & Adams, C. (2020). Spatial visualization of geochemical data: application to the Chichinautzin volcanic field, Mexico. In Updates in Volcanology-Transdisciplinary Nature of Volcano Science. IntechOpen.
72. Robidoux, P., Pastén, D., Levresse, G., Diaz, G., & Paredes, D. (2021). Volatile content implications of increasing explosivity of the strombolian eruptive style along the fracture opening on the NE Villarrica Flank: Minor eruptive centers in the Los Nevados Group 2. Geosciences, 11(8), 309.
73. Rose-Koga, E.F., Bouvier, A.S., Gaetani, G.A., Wallace, P.J., Allison, C.M., Andrys, J.A., De La Torre, C.A., Barth, A., Bodnar, R.J., Gartner, A.B. and Butters, D. (2021). Silicate melt inclusions in the new millennium: a review of recommended practices for preparation, analysis, and data presentation. Chemical Geology, 570, 120145.
74. Roedder, E. (1984). Volume 12: fluid inclusions. Reviews in mineralogy, 12, 644.
75. Romero, J.E., Morgado, E., Pisello, A., Boschetty, F., Petrelli, M., Cáceres, F., Alam, M.A., Polacci, M., Palma, J.L., Arzilli, F. and Vera, F. (2022). Pre-eruptive Conditions of the 3 March 2015 Lava Fountain of Villarrica Volcano (Southern

Andes). Bulletin of Volcanology, 85(1), 2.

76. Roulleau, E., Tardani, D., Sano, Y., Takahata, N., Vinet, N., Bravo, F., Muñoz, C. and Sanchez, J., (2016). New insight from noble gas and stable isotopes of geothermal/hydrothermal fluids at Caviahue-Copahue Volcanic Complex: Boiling steam separation and water-rock interaction at shallow depth. Journal of Volcanology and Geothermal Research, 328, 70-83.
77. Ruth, D. C., Cottrell, E., Cortes, J. A., Kelley, K. A., & Calder, E. S. (2016). From passive degassing to violent Strombolian eruption: the case of the 2008 eruption of Llaima volcano, Chile. Journal of Petrology, 57(9), 1833-1864.
78. Sano, Y., & Marty, B. (1995). Origin of carbon in fumarolic gas from island arcs. Chemical Geology, 119(1-4), 265-274.
79. Sano, Y., & Fischer, T. P. (2013). The analysis and interpretation of noble gases in modern hydrothermal systems. The noble gases as geochemical tracers, 249-317.
80. Silva Parejas, C., Druitt, T. H., Robin, C., Moreno, H., & Naranjo, J. A. (2010). The Holocene Pucón eruption of Volcán Villarrica, Chile: deposit architecture and eruption chronology. Bulletin of volcanology, 72, 677-692.
81. Smith, I. E. M., & Németh, K. (2017). Source to surface model of monogenetic volcanism: a critical review. Geological Society, London, Special Publications, 446(1), 1-28.
82. Stern, C. R. (2004). Active Andean volcanism: its geologic and tectonic setting. Revista geológica de Chile, 31(2), 161-206. Revista Geológica de Chile, Vol. 31, No. 2, p http://dx.doi.org/10.4067/S0716-02082004000200001
83. Stix, J. (2007). Stability and instability of quiescently active volcanoes: The case of Masaya, Nicaragua. Geology, 35(6), 535-538.
84. Tassara, A., & Echaurren, A. (2012). Anatomy of the Andean subduction zone: three-dimensional density model upgraded and compared against global-scale models. Geophysical Journal International, 189(1), 161-168.
85. Valentine, G. A., & Connor, C. B. (2015). Basaltic volcanic fields. In The encyclopedia of volcanoes (pp. 423-439). Academic Press.
86. Wallace, P. J., Plank, T., Bodnar, R. J., Gaetani, G. A., & Shea, T. (2021). Olivine-hosted melt inclusions: a microscopic perspective on a complex magmatic world. Annual Review of Earth and Planetary Sciences, 49, 465-494.
87. Watt, S. F., Pyle, D. M., & Mather, T. A. (2013). The volcanic response to deglaciation: Evidence from glaciated arcs and a reassessment of global eruption records. Earth-Science Reviews, 122, 77-102.
88. Wieser, P. E., Turner, S. J., Mather, T. A., Pyle, D. M., Savov, I. P., & Orozco, G. (2019). New constraints from Central Chile on the origins of enriched continental compositions in thick-crusted arc magmas. Geochimica et Cosmochimica Acta, 267, 51-74.
89. Witter, J. B., Kress, V. C., Delmelle, P., & Stix, J. (2004). Volatile degassing, petrology, and magma dynamics of the Villarrica Lava Lake, Southern Chile. Journal of volcanology and geothermal research, 134(4), 303-337.
90. Zellmer, G. F., Edmonds, M., & Straub, S. M. (2015). Volatiles in subduction zone magmatism. Geological Society, London, Special Publications, 410(1), 1-17.

Figure 1

Click here to access/download;Figure;Figure 1.jpg

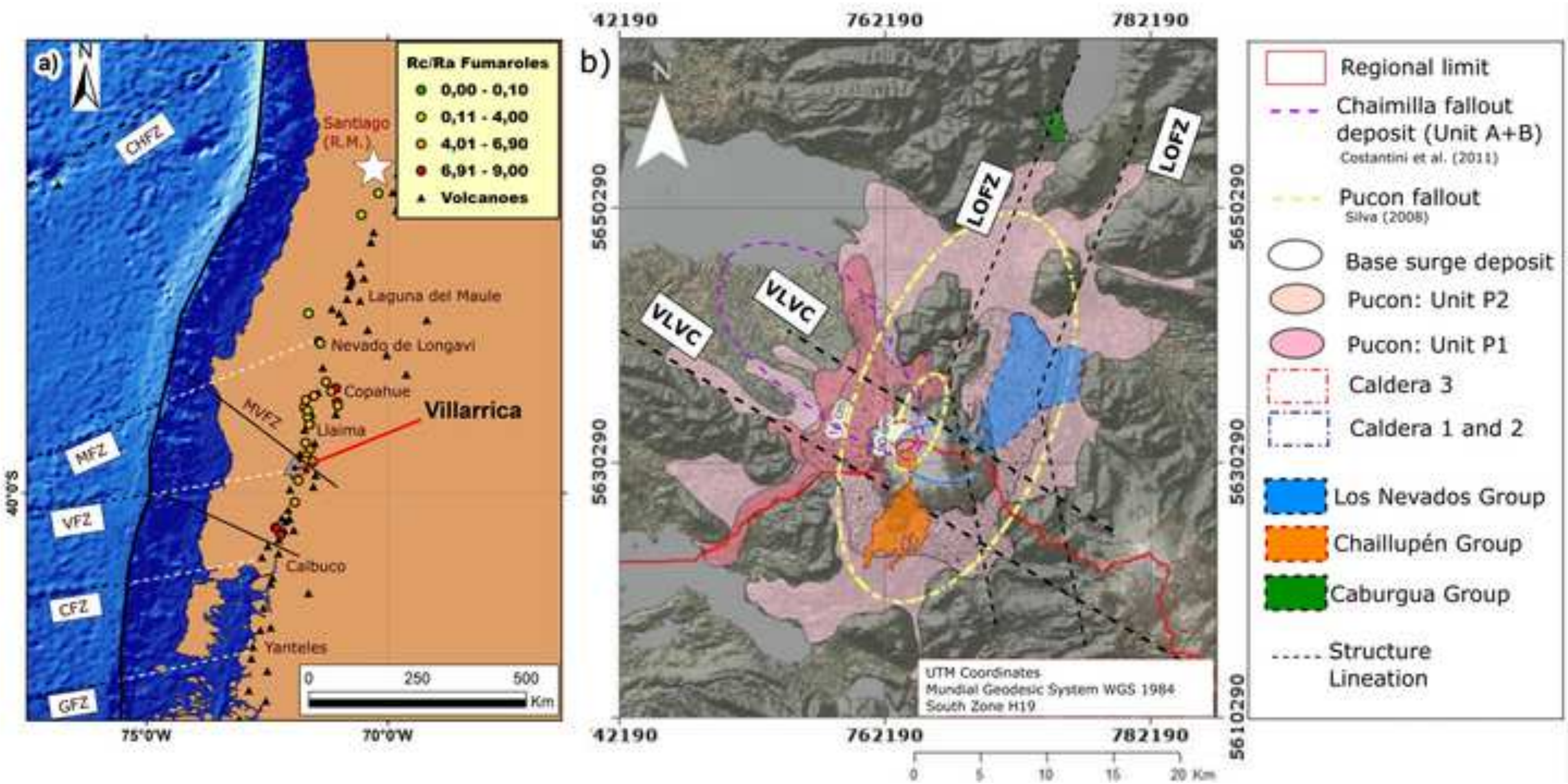

Figure 2

Click here to access/download;Figure;Figure 2.jpg

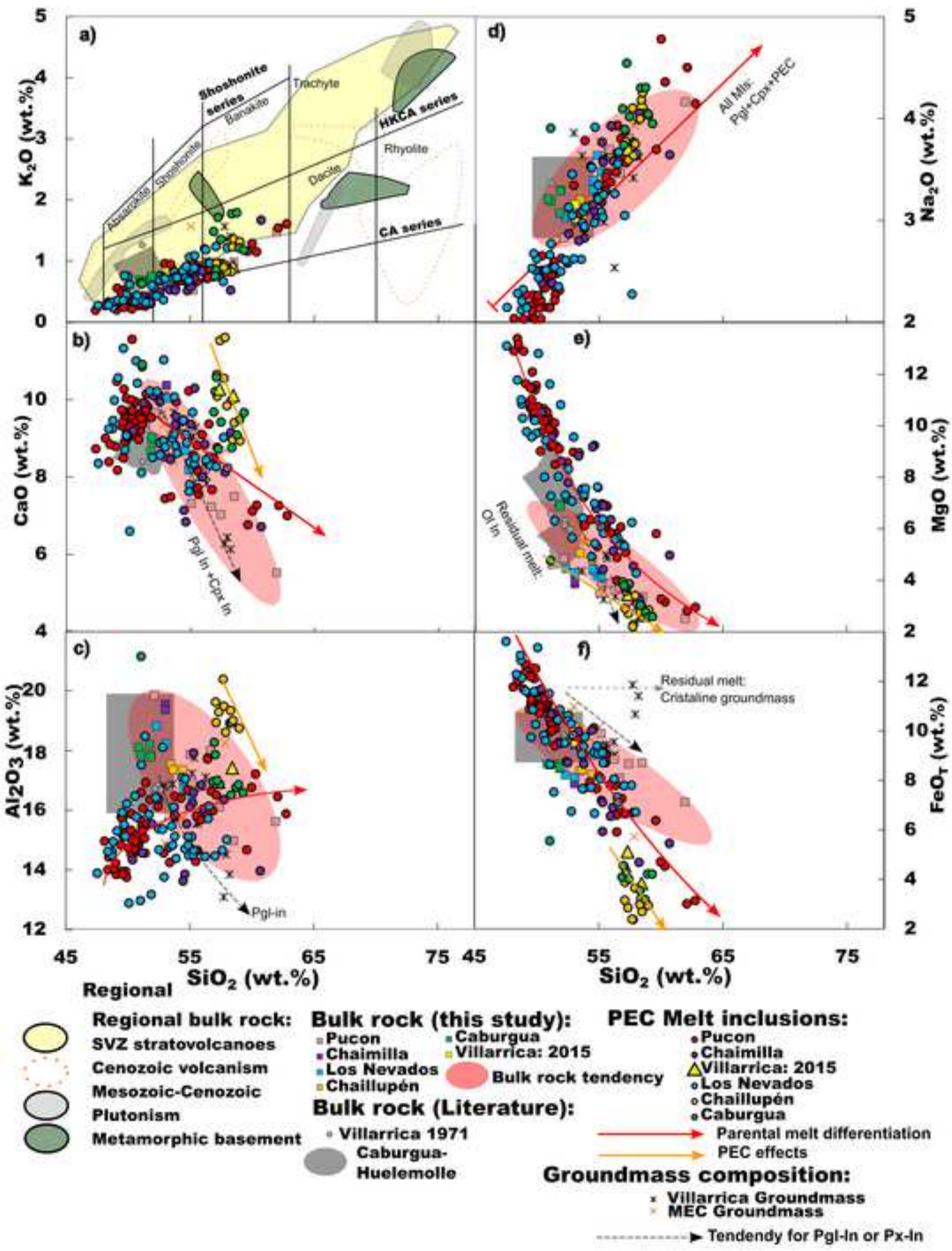

Figure 3 Click here to access/download;Figure;Figure 3.jpg

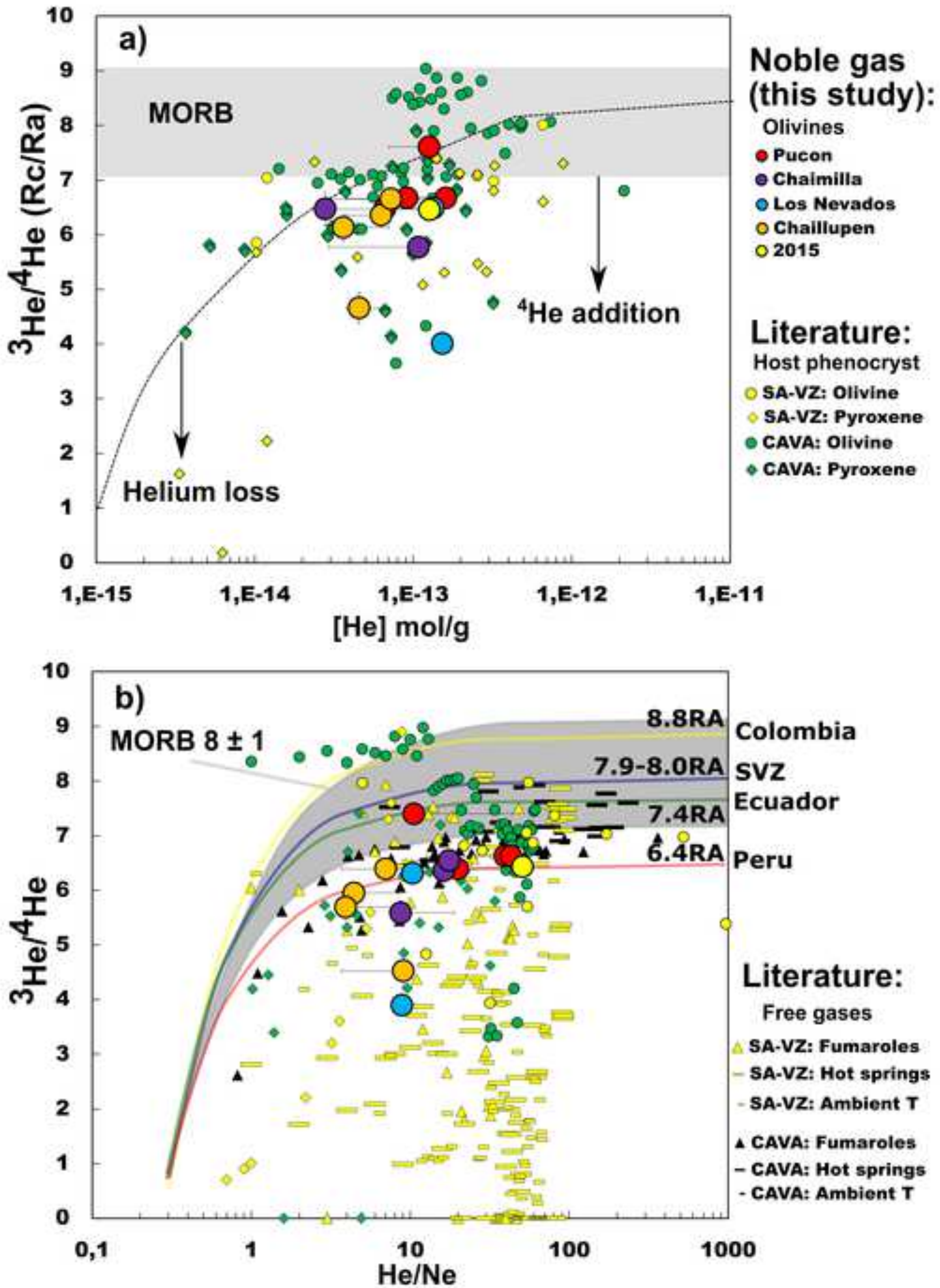

Figure 4 Click here to access/download;Figure;Figure 4.jpg

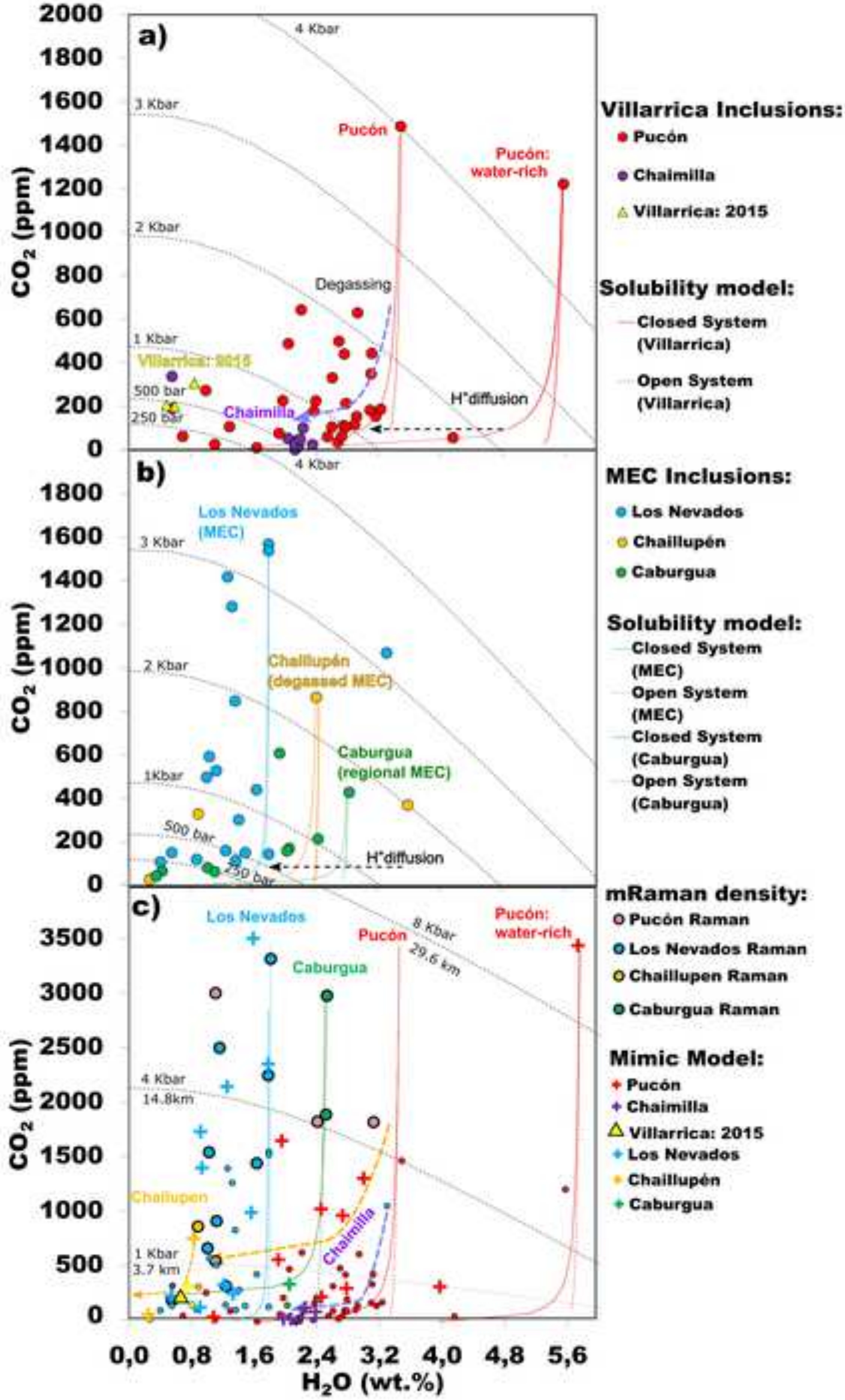

Figure 5

Click here to access/download;Figure;Figure 5.jpg

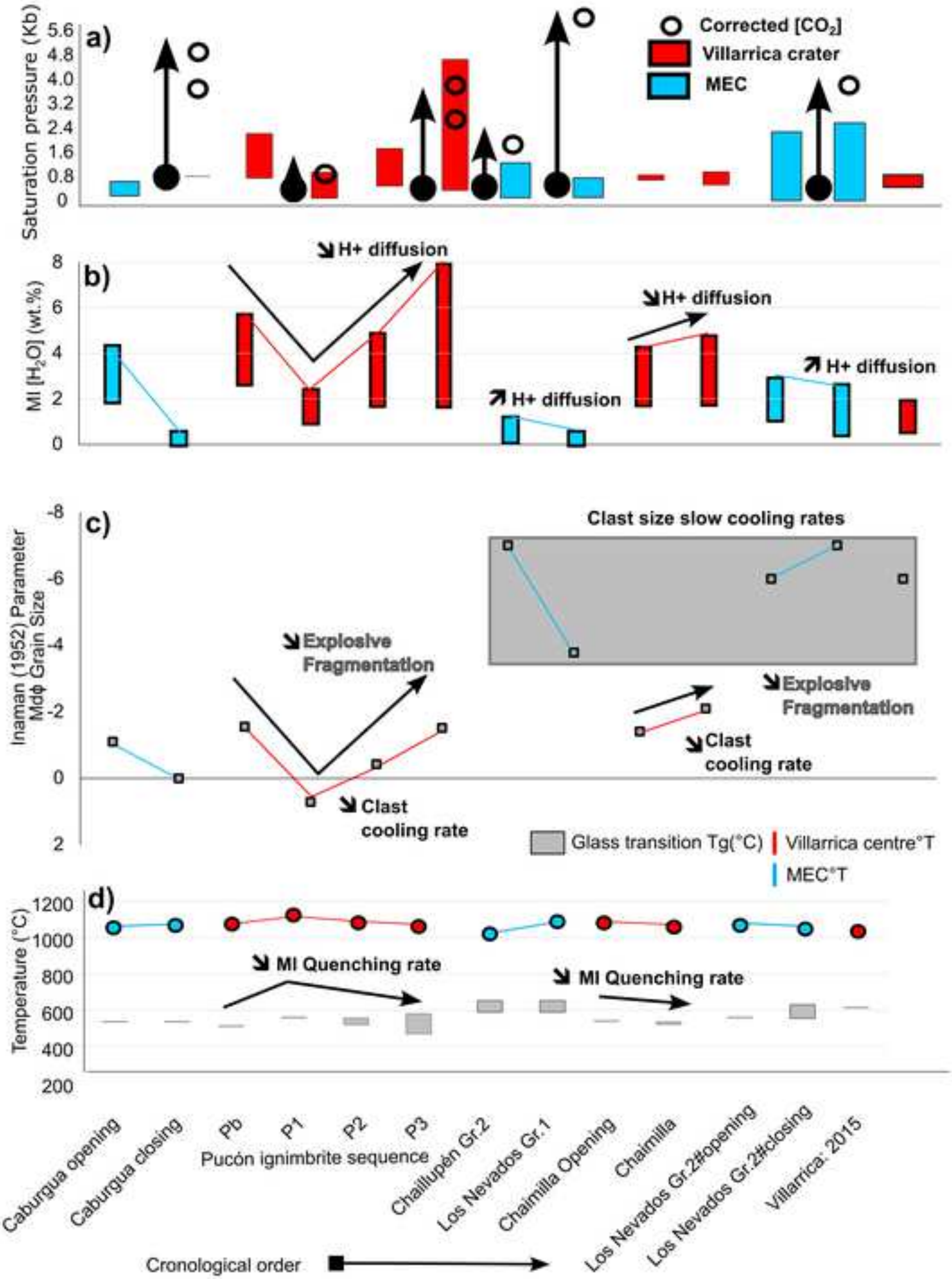

Figure 6

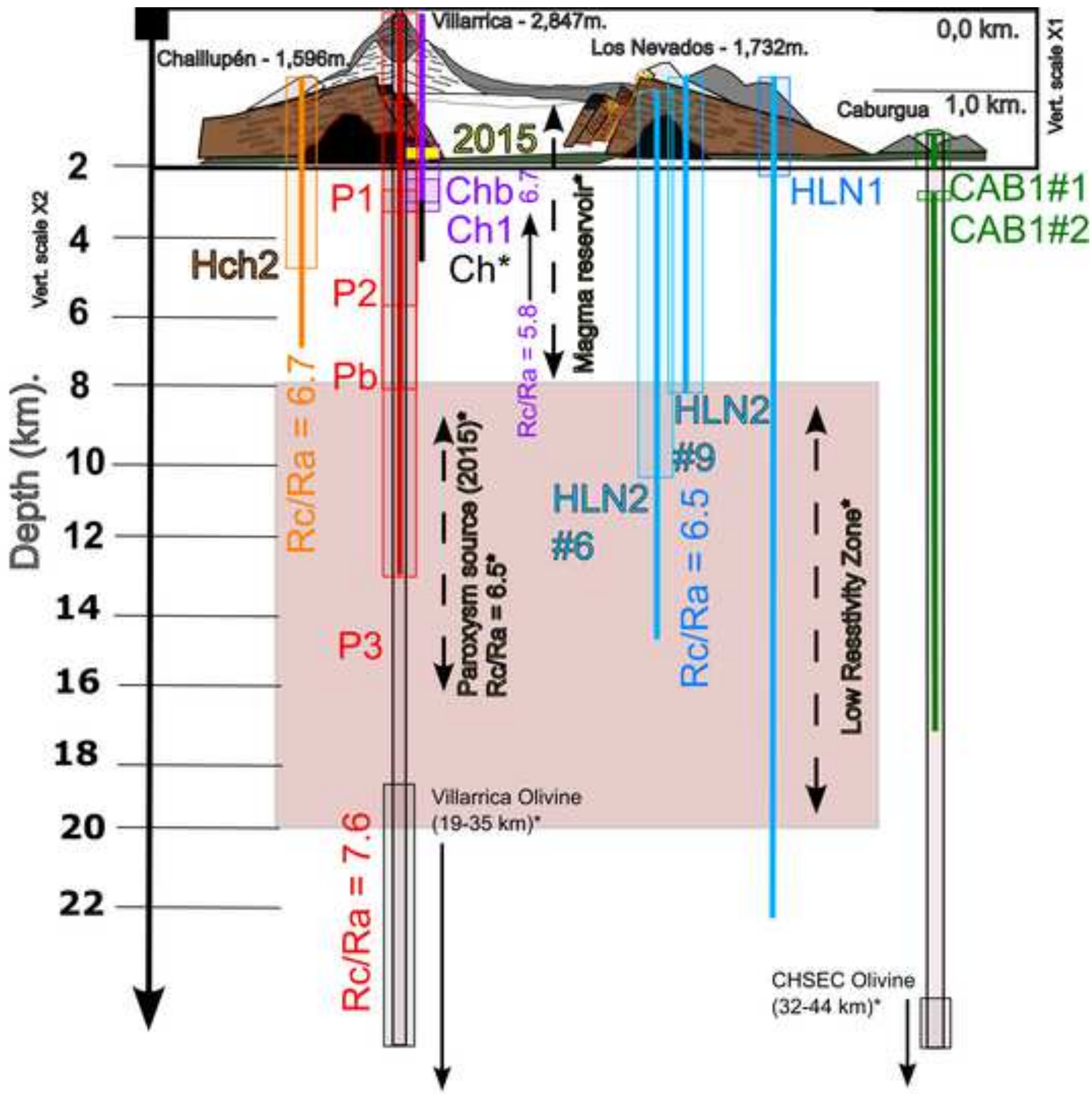

Villarrica - 2,847m.
Chaillupén - 1,596m.
Los Nevados - 1,732m.
0,0 km.
1,0 km.
Caburgua
Vert. scale X1
2015
Vert. scale X2
Depth (km).
2
4
6
8
10
12
14
16
18
20
22
Hch2
Rc/Ra = 6.7
P1
P2
Pb
P3
Rc/Ra = 7.6
Chb
Ch1
Ch*
6.7
Rc/Ra = 5.8
Magma reservoir*
Paroxysm source (2015)*
Rc/Ra = 6.5*
HLN2 #6
HLN2 #9
Rc/Ra = 6.5
HLN1
Low Resistivity Zone*
CAB1#1
CAB1#2
Villarrica Olivine
(19-35 km)*
CHSEC Olivine
(32-44 km)*

Figure 7

Click here to access/download;Figure;Figure 7.jpg

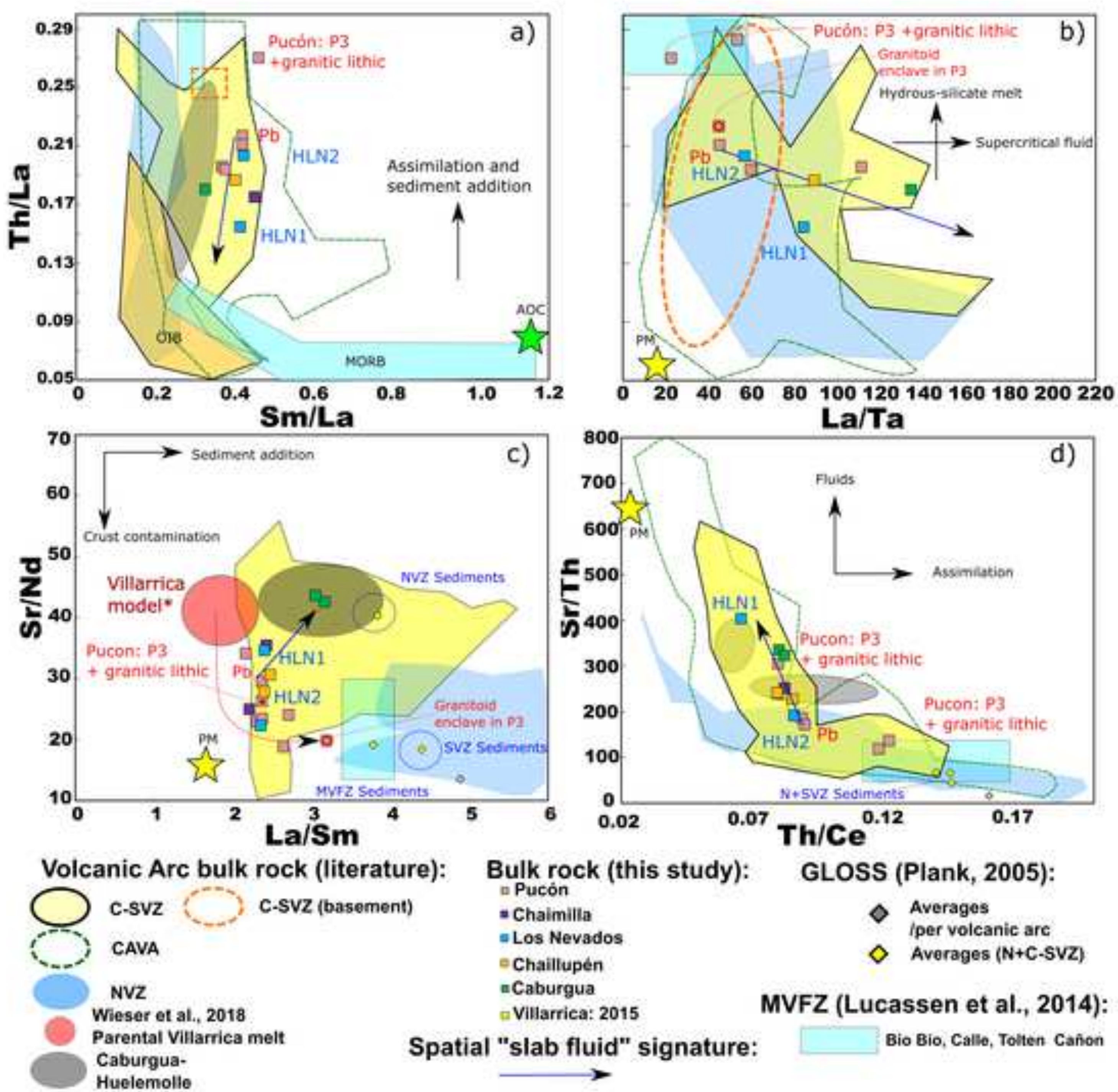

Figure 8

Click here to access/download;Figure;Figure 8.jpg

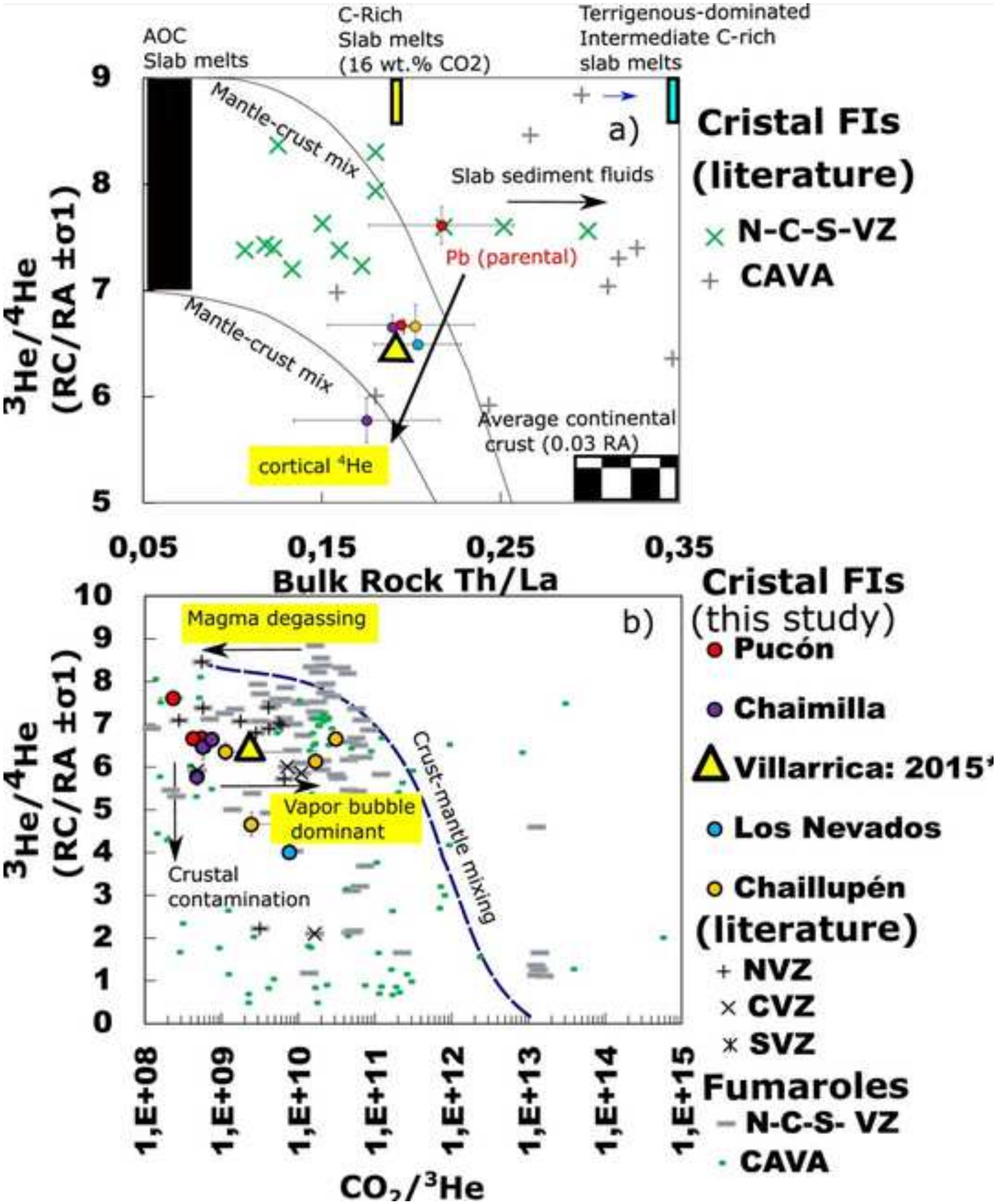

Figure 9

Click here to access/download;Figure;Figure 9.jpg

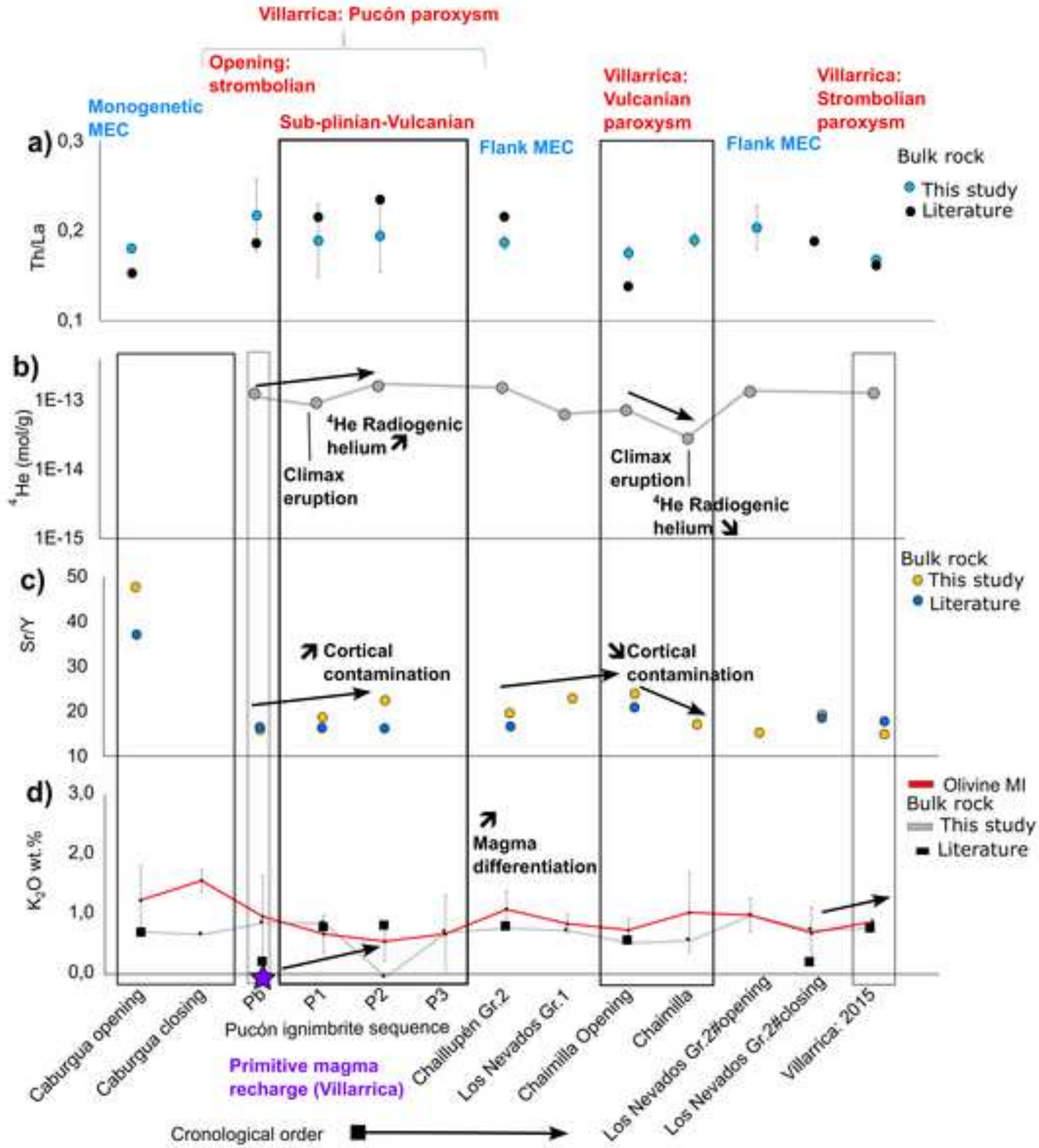

Table 1 Click here to access/download;Table;Table1.xlsx

Sample	Deposit
TVP-10E	Fall deposit
Villa_tvp03x_mic[1]	Piroclastic flow deposit rich in juvenile
TUPI-5AB	Piroclastic flow deposit rich in lithic
TUPI-5C	Piroclastic flow deposit rich in lithic
TUP 06-B	Fallout deposit
TUP 06-C	Fallout deposit
TUP 06-D	Fallout deposit
Villa_p2015+m2015; 2015_B[2]	Piroclast - Scoriaceous bomb
HLN1A3D[3,4]	Piroclast - Scoriaceous bomb
HLN2A6F[3,4]	Piroclast - Scoriaceous fusiform bomb
HLN2A9[3,4]	Piroclast - Scoriaceous lapilli-bomb
HCH-2A5[5]	Piroclast - Scoriaceous fusiform bomb
Villarica HCH2A1[2,5]	Piroclast - Scoriaceous fusiform bomb
Villarica HCH2A4C[2,5]	Lava core
PR1_cab1bc2xmi1[5]	Fall deposit

Reference list:

1 Gloria Estefanía Díaz Miranda. Universidad Mayor. Mei

2 Lages, J., Rizzo, A. L., Aiuppa, A., Robidoux, P., Aguila

3 Daniela Patricia Pastén Muñoz. Universidad Mayor. Me

4 Robidoux, P., Pastén, D., Levresse, G., Diaz, G., & Pai

5 Aaron Matías Sancho Escalante. Universidad Mayor. M

6 Pioli, L., Scalisi, L., Costantini, L., Di Muro, A., Bonadoi

Unit Asociation	Fisher (1966)
Villarrica: Pucon Pb	Toba Lapilli
Villarrica: Pucon P1	Toba Lapilli
Villarrica: Pucon P2-P3	Toba Lapilli
Villarrica: Pucon P2-P3	Toba Lapilli
Villarrica: Chaimilla Lower Sequence (18% lithics= A+B)	Toba Lapilli Breccia
Villarrica: Chaimilla Lower Sequence (18% lithics= A+B)	Toba Lapilli Breccia
Villarrica: Chaimilla Lower Sequence (B-C)[6]	Toba Lapilli Breccia
Villarrica: March, 2015	Breccia lapilli
Los Nevados Gr. 1	Lapilli breccia
Los Nevados Gr. 2	Lapilli breccia
Los Nevados Gr. 2	Lapilli breccia
Chaillupén Gr. 2	-
Chaillupén Gr. 2	-
Chaillupén Gr. 2	-
Caburgua Cone 1	Toba

moria de Licenciatura: “Condiciones Pre-Eruptivas De Las Últimas Etapas Del Evento Pucón, Volcán Villarrica (39.5°S); An

ar Contreras, R., Apaza Choquehuayta, F. E., & Masías Alvarez, P. J. (2021). Crustal controls on light noble gas isotope va

emoria de Licenciatura: “Relación entre Estilos de Desgasificación y Eruptivos en los Centros Eruptivos Menores Los Nevad

redes, D. (2021). Volatile content implications of increasing explosivity of the strombolian eruptive style along the fracture o

Memoria de Licenciatura: “Rol e implicancias de los volátiles magmáticos en las condiciones pre-eruptivas de los centros er

nna, C., & Clavero, J. (2015). Explosive style, magma degassing and evolution in the Chaimilla eruption, Villarrica volcano,

White y Houghton (2006)	Graphical Std. (σφ) Sorting	Inaman (1952) Parameter (Mdϕ) : Grain Size
Lithic Toba	1.45	-1.55
Vitric Toba	2.68	0.72
Lithic Toba	2.19	-0.43
Lithic Toba	1.35	-1.52
Lithic Toba with 18%lithics	1.1	-1.41
Lithic Toba with 18%lithics	1.1	-1.40
Lithic Toba	0.97	-2.10
Vitric Toba	-	-6.00
Vitric Toba	3.30	-3.78
Vitric Toba	-	-7.00
Vitric Toba	-	-6.00
-	3.50	-7.00
-	3.30	-7.00
-	-	-
Vitric Toba	-0.37	-1.10

ıdes Del Sur". (November 2019). Supervisor: Prof. Philippe Robidoux

riability along the Andean Volcanic Arc.

dos, Andes del Sur". (October 2019). Supervisor: Prof. Philippe Robidoux, Review Commission

ɔening on the NE Villarrica Flank: Minor eruptive centers in the Los Nevados Group 2. Geosciences, 11(8), 309.

uptivos menores Caburgua y Chaillupén, Andes del Sur". (October 2019). Supervisor: Prof. Philippe Robidoux

Southern Andes. Bulletin of Volcanology, 77, 1-14.

Table 2

Click here to access/download;Table;Table2.xlsx

Villarrica Eruptive Centre	Granulometry	BR	Olivine Populations	Noble Gas
Table(s)	-	Table A.2	Table A.3, A.11	Table A.10
Appendix equivalent	-	B	D, L	K
Figure(s)	Fig. SM1	Fig.7,8, A.1, A.7, A.8		Fig.3,8, A.7
Appendix equivalent	A			
Erupton Series (#analysis)				
Pucón ignimbrite (Pb)	1	3	1	2
Pucón ignimbrite (P1)	4	1	1	1
Pucón ignimbrite (P2)	3	2	1	1
Pucón ignimbrite (P3)	2	3	1	0
Chaimilla (A+B) Opening	2	1	1	1
Chaimilla (B+C)	1	1	2	2
Villarrica: March, 2015	2	2	1	1*
Los Nevados Gr.1	3	3	1	1
Los Nevados Gr.2	3	3	2	1
Chaillupén Gr.2	2	3	4	2+2*
Caburgua	10	5	1	0

*Lages, J., Rizzo, A. L., Aiuppa, A., Robidoux, P., Aguilar Contreras, R., Apaza Choquehuayta, F. E.,

Olivine-EMPA	mFTIR	SIMS	MI-EMPA	mRaman	Mimic
Table A.4	Table A.5, A.7	Table A.6, A.7	Table A.8	Table A.9	Table A.8
E	F, H	G, H	I	J	I
Fig.A.2	Fig.4, A.4, A.5, A.6	Fig. A.3, A.4, A.5, A.6	Fig.2, Fig. SM2		
			A		
37	43	21	34	0	1
10	2	2	4	5	1
10	22	11	10	0	3
24	35	0	19	8	5
6	3	5	6	0	1
31	10	10	16	0	4
2	7	1	2	0	1
6	2	3	6	1	0
23	-	6	40	8	10
11	12	0	10	1	2
13	26	3	13	8	2

& Masías Alvarez, P. J. (2021). Crustal controls on light noble gas isotope variability along the Ande

an Volcanic Arc. Geochemical Perspectives Letters, uri: issn: 2410339X.

Appendix B – Table A.1

Click here to access/download

Supplementary material/Appendix (Files for online publication only)

Appendix B.xlsx

Appendix C – Table A.2

Appendix D – Table A.3

Click here to access/download

Supplementary material/Appendix (Files for online publication only)

Appendix D.xlsx

Appendix E – Table A.4

Click here to access/download

Supplementary material/Appendix (Files for online publication only)

Appendix E.xlsx

Appendix F – Table A.5

Click here to access/download
Supplementary material/Appendix (Files for online publication only)
Appendix F.xlsx

Appendix H – Table A.7

Click here to access/download
Supplementary material/Appendix (Files for online publication only)
Appendix H.xlsx

Appendix I – Table A.8

Click here to access/download
Supplementary material/Appendix (Files for online publication only)
Appendix I.xlsx

Appendix J – Table A.9

Click here to access/download
Supplementary material/Appendix (Files for online publication only)
Appendix J.xlsx

Appendix K – Table A.10

Click here to access/download
Supplementary material/Appendix (Files for online publication only)
Appendix K.xlsx

Click here to access/download
Supplementary material/Appendix (Files for online publication only)
Appendix L.xlsx

Appendix M – Figure A.1

Click here to access/download

Supplementary material/Appendix (Files for online publication only)

Appendix M.jpg

Appendix N – Figure A.2

Declaration of interests

☒The authors declare that they have no known competing financial interests or personal relationships that could have appeared to influence the work reported in this paper.

☐The authors declare the following financial interests/personal relationships which may be considered as potential competing interests: